Supplementary information

Breaking current limitation of electrochemical CO_2 reduction via silica-hydroxide cycle

Chulwan Lim[a,b], Sangkuk Kim[a,c], Ji Hwan Song[a], Man Ho Han[a], Young-Jin Ko[a], Kwan-Young Lee[b], Jae-Young Choi[d,e], Woong Hee Lee[a,*] and Hyung-Suk Oh[a,d,e,*]

[a] *Clean Energy Research Center, Korea Institute of Science and Technology (KIST), Hwarang-ro 14-gil 5, Seongbuk-gu, Seoul 02792, Republic of Korea*

[b] *Department of Chemical and Biological Engineering, Korea University, 145 Anam-ro, Seongbuk-gu, Seoul, 02841 Republic of Korea*

[c] *Hydrogen and Low-Carbon Energy R&D laboratories, POSCO HOLDINGS, 67 Cheongam-ro, Nam-gu, Pohang-si, Gyeongsangbuk-do, 37673, Republic of Korea*

[d] *School of Advanced Materials Science & Engineering, Sungkyunkwan University (SKKU), Suwon, 16419, Republic of Korea*

[e] *KIST-SKKU Carbon-Neutral Research Center, Sungkyunkwan University (SKKU), Suwon 16419, Republic of Korea*

Note S1. Analysis of CO_2 cross-over-through the AEM

The CO_2RR and the HER produce OH^- anions at the cathode under both basic and neutral conditions (1). These anions react with CO_2 to produce HCO_3^- and CO_3^{2-} anions (2). The transport of these charged species through the AEM originates from cathodic CO_2 (HCO_3^- and CO_3^{2-}), culminating in their release as CO_2 over the anode (3).

Release of OH^- at the Cathode (1)

$CO_2 + 2e^- + H_2O \rightarrow CO + 2OH^-$

$CO_2 + 2e^- + H_2O \rightarrow HCOO^- + OH^-$

$2H_2O + 2e^- \rightarrow H_2 + 2OH^-$

Neutralization of CO_2 at the Cathode (2)

$CO_2 + OH^- \rightarrow HCO_3^-$

$HCO_3^- + OH^- \rightarrow CO_3^{2-} + H_2O$

Gas Evolution (O_2 and CO_2) at the Anode (3)

$2H_2O \rightarrow O_2 + 4H^+ + 4e^-$

$HCO_3^- + H^+ \rightarrow CO_2 + H_2O$

$CO_3^{2-} + 2H^+ \rightarrow CO_2 + H_2O$

The analysis of the anodic CO_2 to O_2 ratio in CO_2RR devices serves as a proxy to determine which species, such as HCO_3^-, CO_3^{2-}, or OH^-, are transferring through the AEM. As all the charges are carried by OH^-, CO_3^{2-}, or HCO_3^- transfer, the CO_2 to O_2 ratio on the anode side will be 0, 2, or 4, respectively. The trap was filled with the electrolyte and purged with Ar gas at a flow rate of 100 sccm at the anode. This trap was then connected to the GC. Peaks representing oxygen (O_2) and carbon dioxide (CO_2) evolution over the anode were captured from the TCD of the GC. The outflowing anodic gas stream was measured using a mass flow meter (Agilent). The CO_2 to O_2 ratio was derived using the peak areas for CO_2 and O_2, along with the measured flow rate at each applied current density.

Note S2. pH calibration

Raman spectroscopy results depicted in Figure S17 (spanning pH 7.5-14, using bicarbonate/carbonate peak ratio calibration) were obtained as follows: Eight distinct vials of KOH solutions were created. To adjust the pH values of these KOH solutions, the purging time with CO_2 (100 ml/min) was varied until each solution achieved its desired pH. This was monitored in real-time using a commercial pH meter. For instance, the initial KOH solution without any CO_2 purging displayed a pH of 14. Purging for 4 min resulted in a pH of 13, while 20 min of purging yielded a pH of 9, and so forth. The eight solutions were adjusted to pH values of 14, 13, 12, 11, 10, 9, 8.5, and 7.5, as shown in Figure S21. After obtaining the Raman data for these solutions, the log-transformed peak area ratio corresponding to bicarbonate species (1013 cm^{-1}) and carbonate species (1064 cm^{-1}) were quantified (Figure S18). Then, as illustrated in Figure S18, the log-transformed relative peak area ratio of carbonate to bicarbonate from the solutions were correlated with their pH values..[1]

However, the calibration using the bicarbonate/carbonate peak ratio is confined to pH values between 7.5 and 11. Consequently, a separate calibration was required for high alkaline media. Raman spectroscopy results for this are shown in Figure S19 (covering pH 13-14, based on relative carbonate Raman peak intensities). To prepare solutions in this pH range, 1 M KOH and 1 M $KHCO_3$ were mixed in varying proportions. It is worth noting that only solutions within the pH range of 13.5 – 14 were used, as those with pH values of 13.0, ~ 13.2 yielded nearly identical Raman spectra. The pH of each solution, post-mixing of 1 M KOH and 1 M $KHCO_3$, was gauged using a commercial pH meter. For a solution with a pH of 14, pure 1 M KOH was employed without adding any 1 M $KHCO_3$. In total, 11 solutions were prepared. Post data collection, log-transformed relative peak area ratio related to carbonate species (1064 cm^{-1}) were normalized as indicated in Figure S20. Only 5 of the 11 solutions were used for calibration (excluding pH values of 13.0 ~13.2). The carbonate Raman peak intensity at pH 13.3 was set as the reference, with an intensity of 1. Subsequent pH values and their relative carbonate Raman peak intensities were correlated.

Another set of results, displayed in Figure S23, focused on K cation concentration and associated Raman peak position shifts. To craft solutions with different K cation concentrations from 1 M to 4 M, the solutions were prepared by mixing 1, 2, 3 and 4 M KOH and 1, 2, 3 and 4 M KHCO3 in specific proportions, respectively. Four distinct solutions were prepared in this manner. After obtaining the Raman data, shifts in the position of peaks corresponding to carbonate species (ranging from 1064 to 1065 cm^{-1}) were determined as outlined in Figure S25. For calibration purposes, the K cation concentrations and the related peak position shifts were correlated.

These calibrations infer that the log-transformed relative peak area ratio is indicative of carbonate concentration, while the carbonate peak shift signifies cation concentration. Both the cation and carbonate concentrations represent the local pH at the electrode. As a result, we can approximately estimate the reaction environment of the electrode under high alkaline conditions using the relative area of the carbonate peak alongside its shift and shows the results in Figure S24 and Table S1.

Note S3. Experiment for observing behavior of SiO_2

To validate the neutralization of local pH by CO_2, we purged CO_2 gas into various alkaline solutions and measured the pH every minute. To determine the effects of the pH of the solutions, we prepared several solutions within a pH range of 10-14. Specifically, the solution denoted as pH 14 was a 1 M KOH solution, while other solutions with pH values of 10, 11, 12, and 13 (± 0.05) were mixtures of 1 M KOH (pH ~14) and 1 M $KHCO_3$ (pH ~8.5), ensuring a consistent amount of total K cations among the solutions. We then purged 9 ml of these solutions with CO_2 gas at a rate of 100 ml/min for 10 min, controlled using a ball flowmeter, while continuously measuring the solution's pH every 60 seconds with a commercial pH meter (Mettler-Toledo).

Additional solutions with pH values of 12 and 13 were prepared using the same protocol. The variation being that 15 mg of pristine SiO_2 powder were dissolved in these solutions with overnight stirring. These were denoted as SiO_2 (pH 13) and SiO_2 (pH 12) as shown in Figure 4A. Changes in the solution pH of these SiO_2-dissolved solutions during CO_2 purging followed the previously mentioned procedures. Furthermore, the inset in Figure 4A displays the change in the amount of OH^- consumed during CO_2 purging in relation to each solution's initial pH values, calculated from the variations in solution pH values during the CO_2 purging. The consumed OH^- relative to the current pH in the Figure 4A inset was calculated using data from Figure 4A and the following equation

$$\text{Consumed } OH^- \text{ (M)} = 10^{current\ pH/15} - 10^{after\ 1\ min\ pH/15}$$

For the Raman spectroscopy depicted in Figure 4D, a reference 1 M $KHCO_3$ solution was manually prepared. To identify any shift in the bicarbonate Raman peaks, a comparison solution was crafted as follows: 90 mg of pristine SiO_2 powder was dissolved in 15 ml of 1 M KOH solution with overnight stirring. The SiO_2-dissolved solution was then purged with 100 ml/min of gaseous CO_2 until the solution pH stabilized around ~7.5, a process that took approximately 2 h to reach saturation. Concurrently, an opaque white gel precipitated within the solution.

For the Raman spectroscopy in Figure 4E, the Raman spectrum of the pristine SiO_2 powder was initially acquired as a reference sample. Subsequently, the Raman spectrum of the centrifuged SiO_2 gel was obtained. First, 90 mg of pristine SiO_2 powder was dissolved in a 15 ml 1 M KOH solution with overnight stirring. This solution was then purged with gaseous CO_2 at 100 ml/min for around 2 h until the pH stabilized at approximately ~7.5. Upon CO_2 saturation, an opaque white gel formed in the solution. This solution, containing the SiO_2 gel, was centrifuged at 12,000 rpm for 10 min to separate

the liquid-solid phases. The resulting opaque SiO_2 gel was washed with D.I. water through subsequent centrifugation processes (12,000 rpm for 10 min, with the SiO_2 gel submerged in 50 ml of D.I. water in a falcon tube), which was repeated three times. Lastly, the obtained SiO_2 gel was dried overnight in a 60 °C convection oven, producing a white powder.

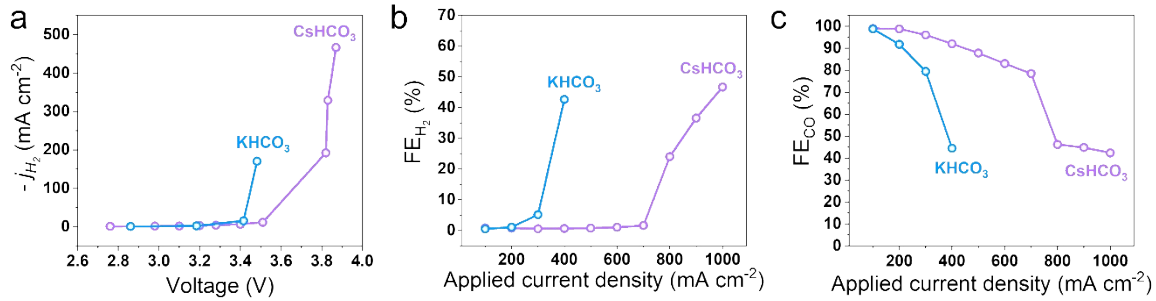

Fig. S1 CO_2RR performance of Ag black in 0.1 M $KHCO_3$ and 0.1 M $CsHCO_3$. (a) H_2 partial current density, (b) H_2 faradaic efficiency and (c) CO faradaic efficiency.

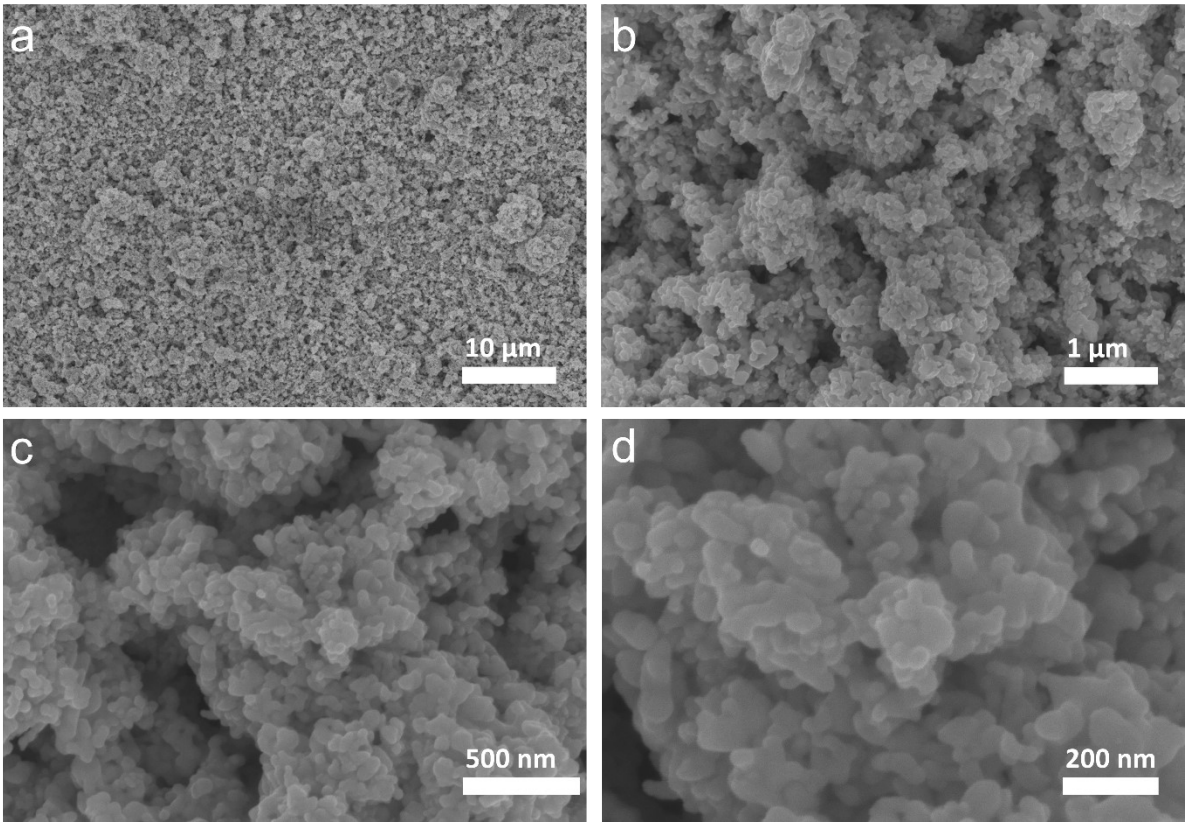

Fig. S2 SEM images of Ag black before CO_2 reduction reaction. (a, b) low-magnification and (c, d) high-magnification.

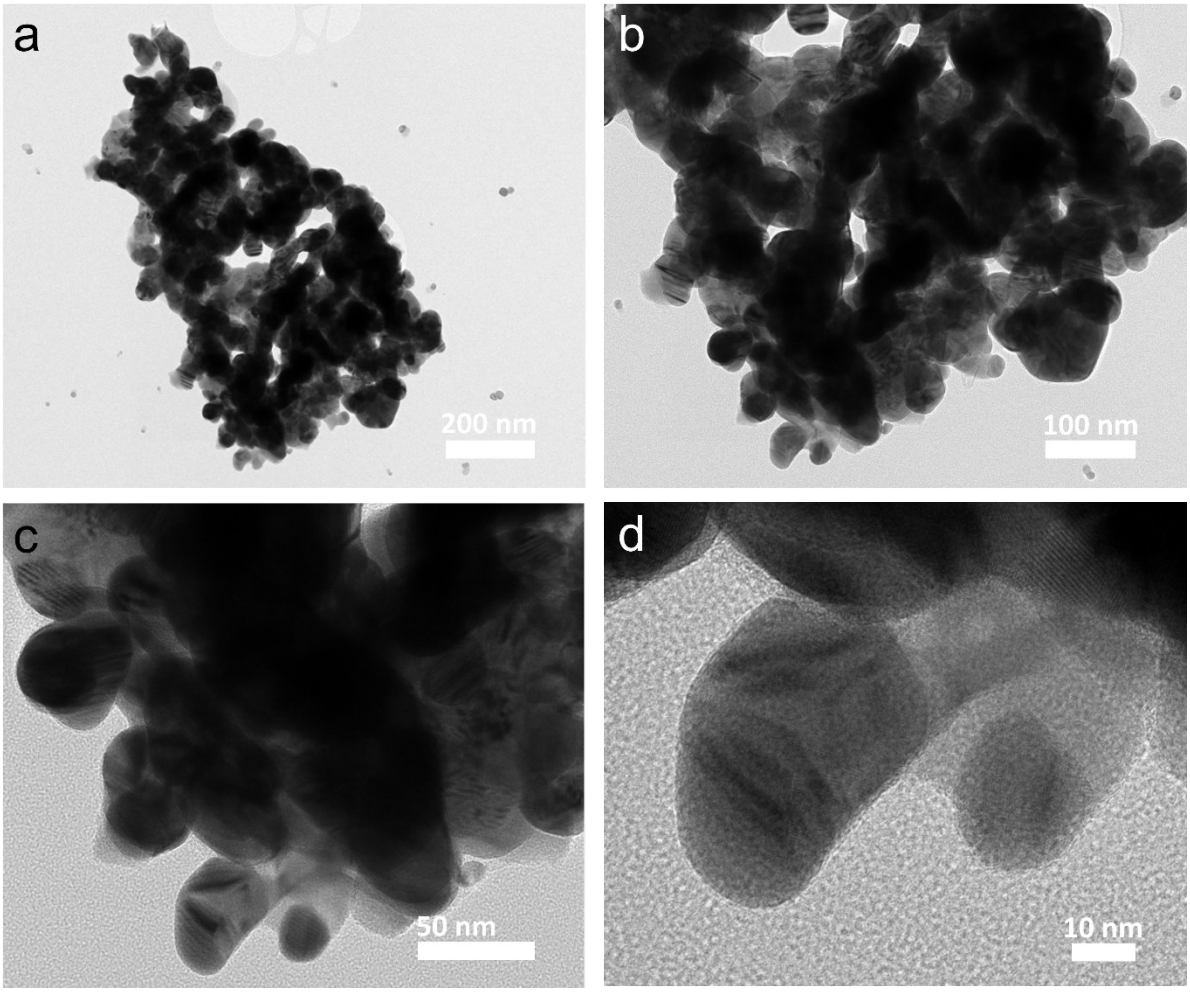

Fig. S3 HR-TEM images of Ag black before CO_2 reduction reaction. (a) low-magnification and (b), (c), (d) high-magnification.

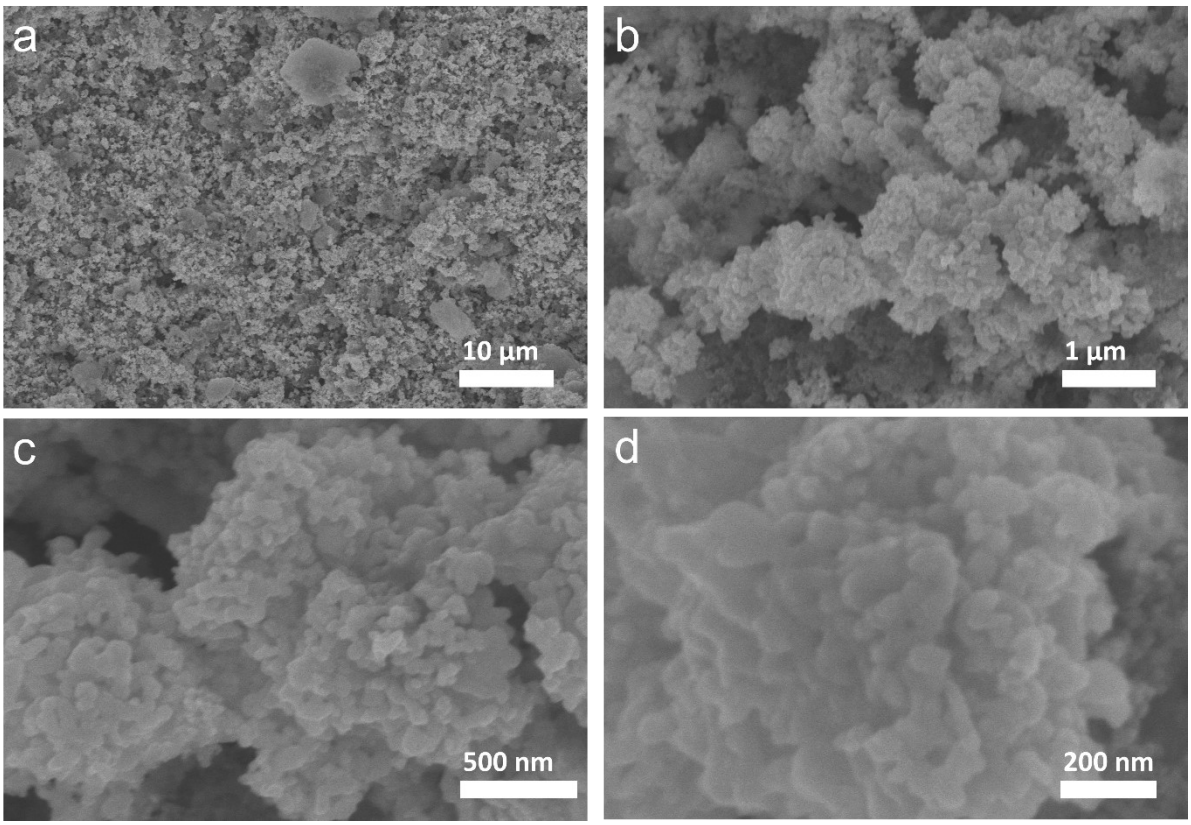

Fig. S4 SEM images of Ag-SiO_2 before CO_2 reduction reaction. (a, b) low-magnification and (c, d) high-magnification.

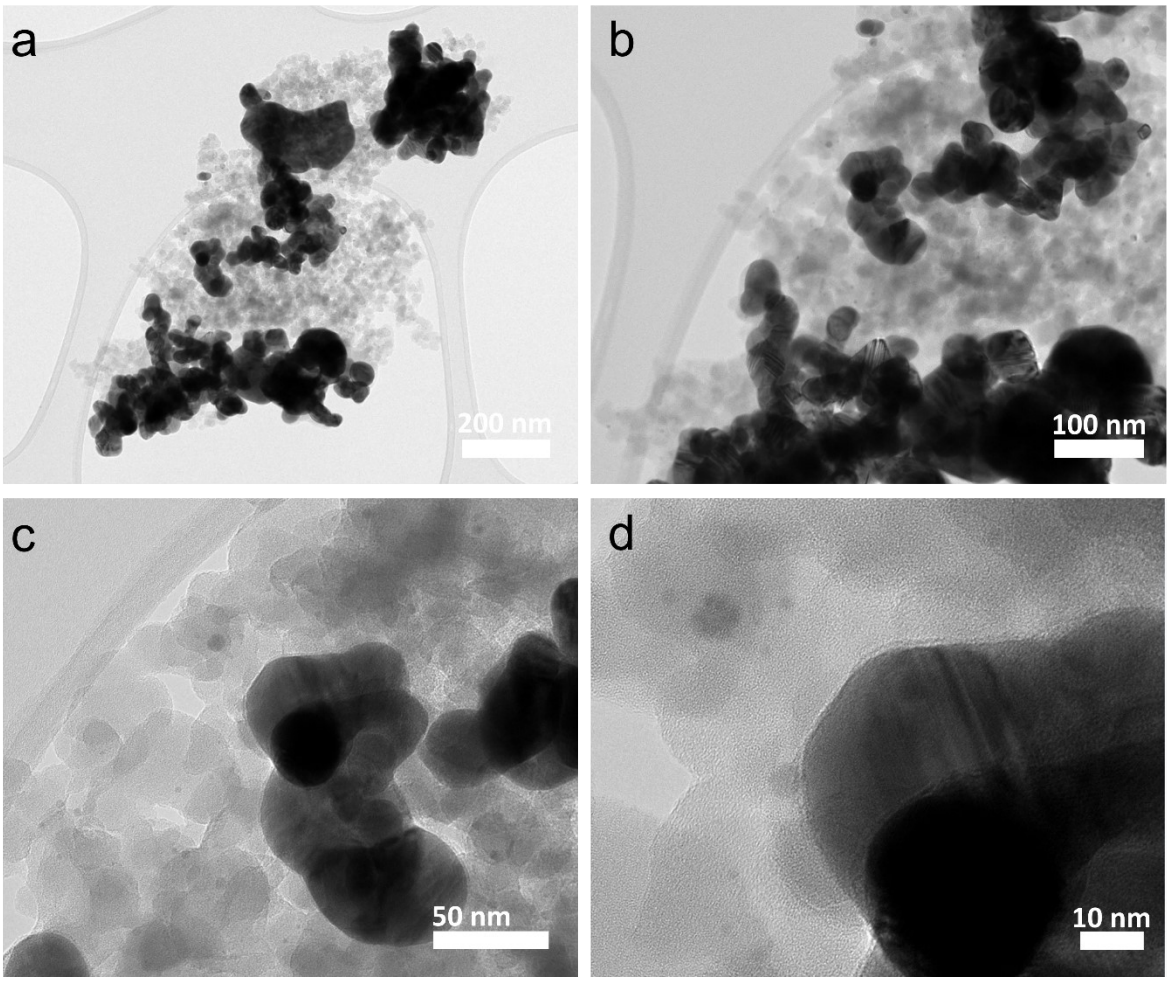

Fig. S5 HR-TEM images of Ag –SiO_2 before CO_2 reduction reaction. (a) low-magnification and (b), (c), (d) high-magnification.

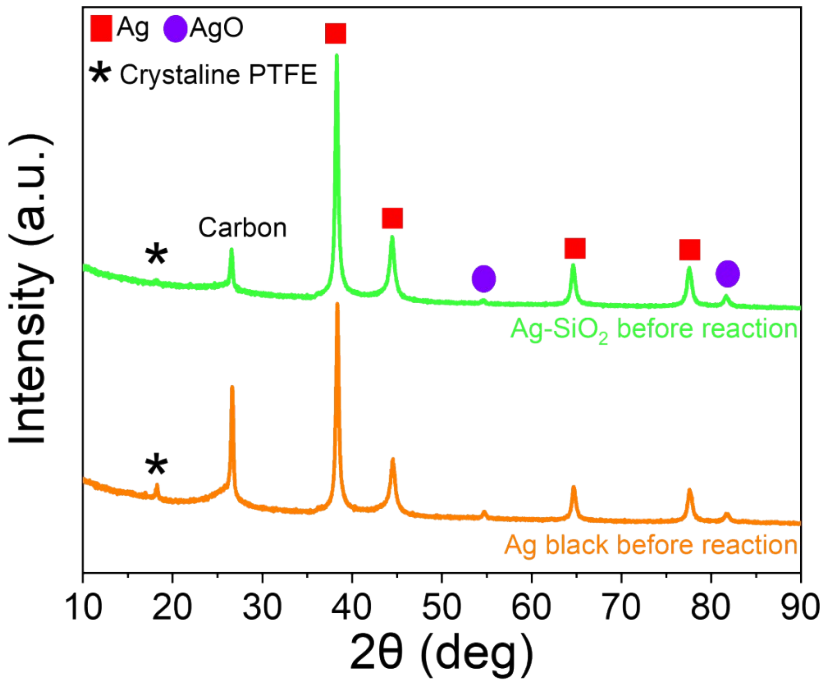

Fig. S6 XRD patterns of Ag black and Ag-SiO_2 before CO_2 reduction reaction

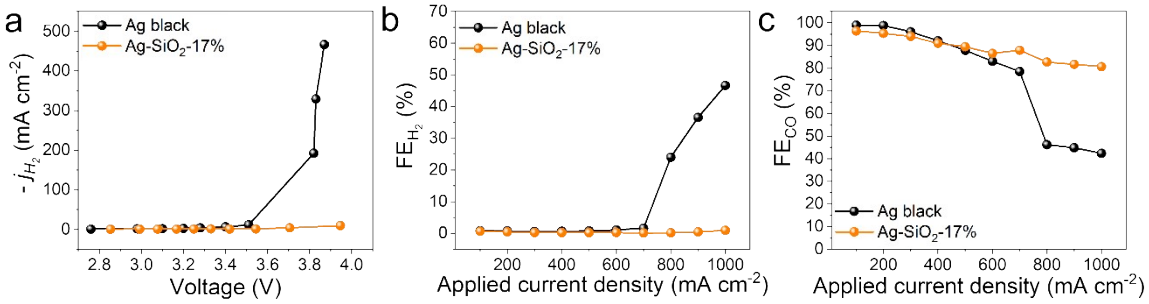

Fig. S7 CO_2RR performance of Ag black and Ag-SiO_2 in 0.1 M $CsHCO_3$. (a) H_2 partial current density, (b) H_2 faradaic efficiency and (c) CO faradaic efficiency.

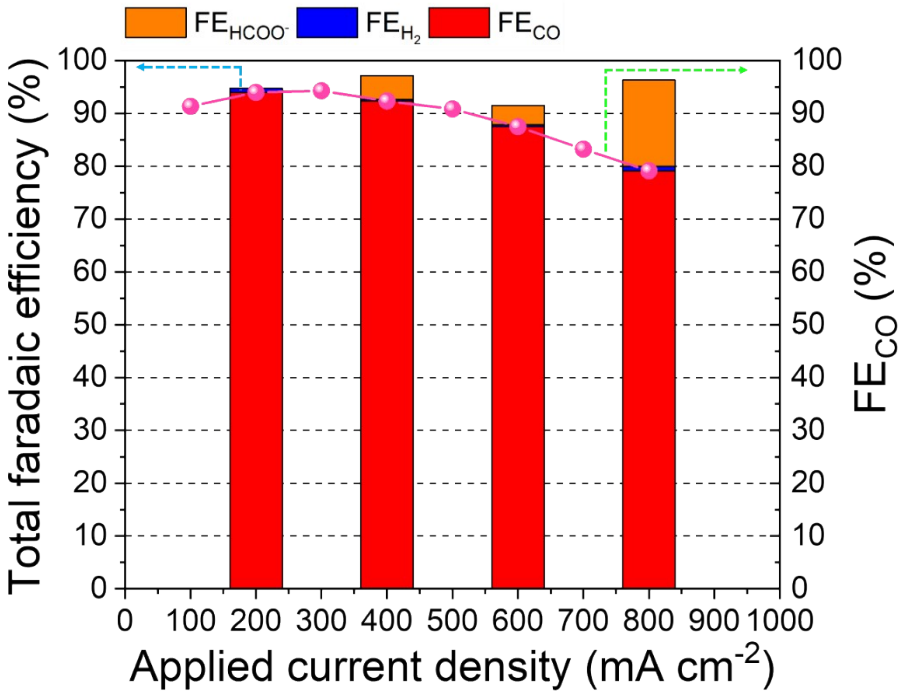

Fig. S8 Total faradaic efficiency of gas product (H_2 and CO) and liquid product (Formate) of Ag-SiO_2 during CO_2RR.

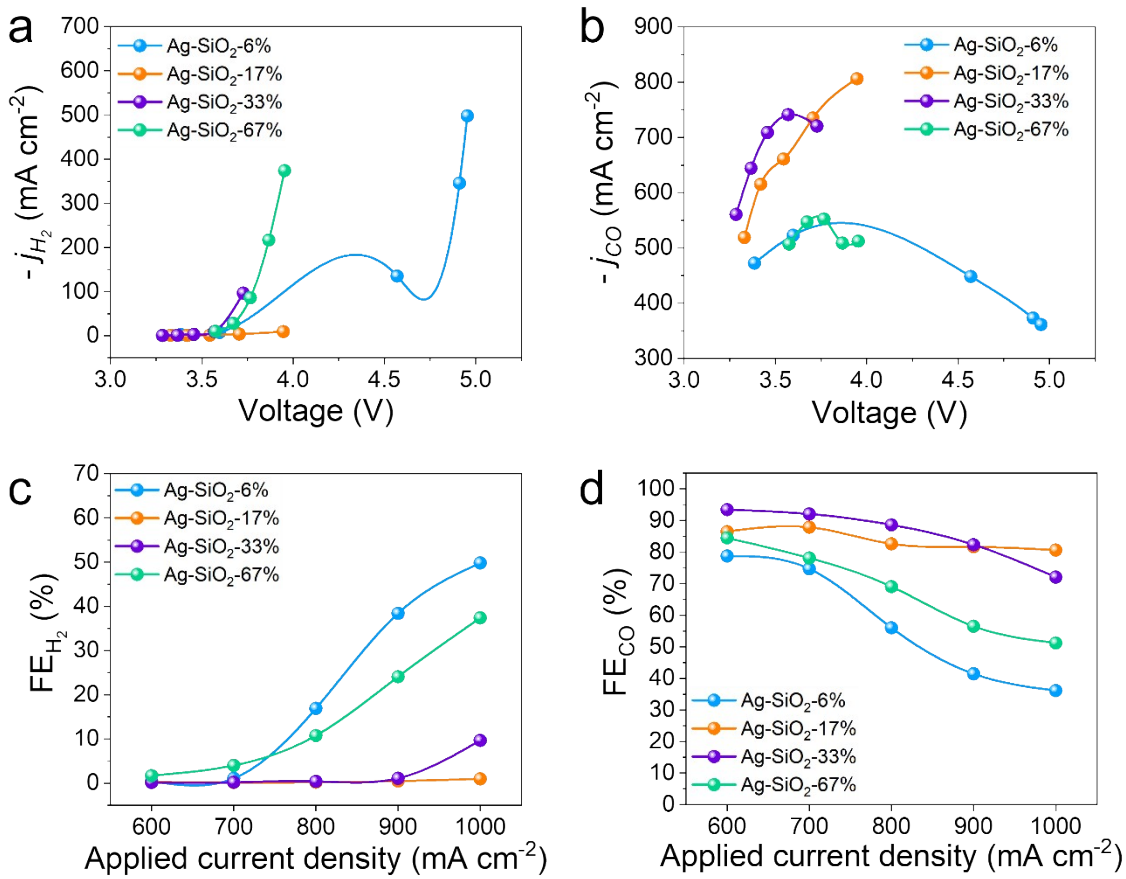

Fig. S9 CO_2RR performance of Ag-SiO_2 with amount of SiO_2 contents. (a) H_2 partial current density, (b) CO partial current density, (C) H_2 faradaic efficiency and (d) CO faradaic efficiency

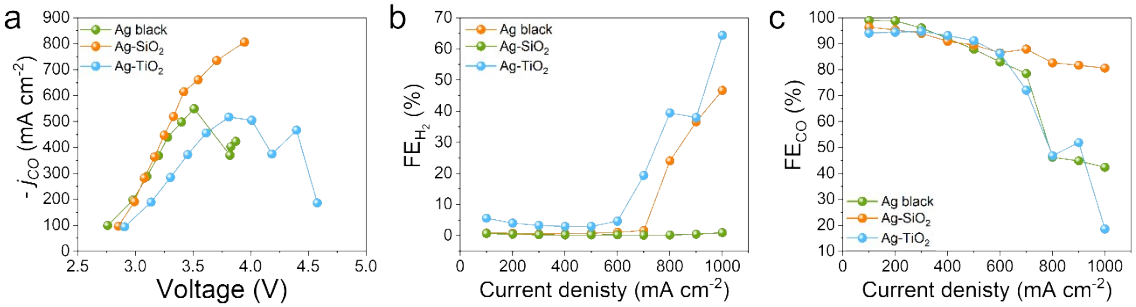

Fig. S10 CO_2RR performance for Ag-TiO_2 and Ag-SiO_2. (a) CO partial current density, (b) H_2 faradaic efficiency and (c) CO faradaic efficiency.

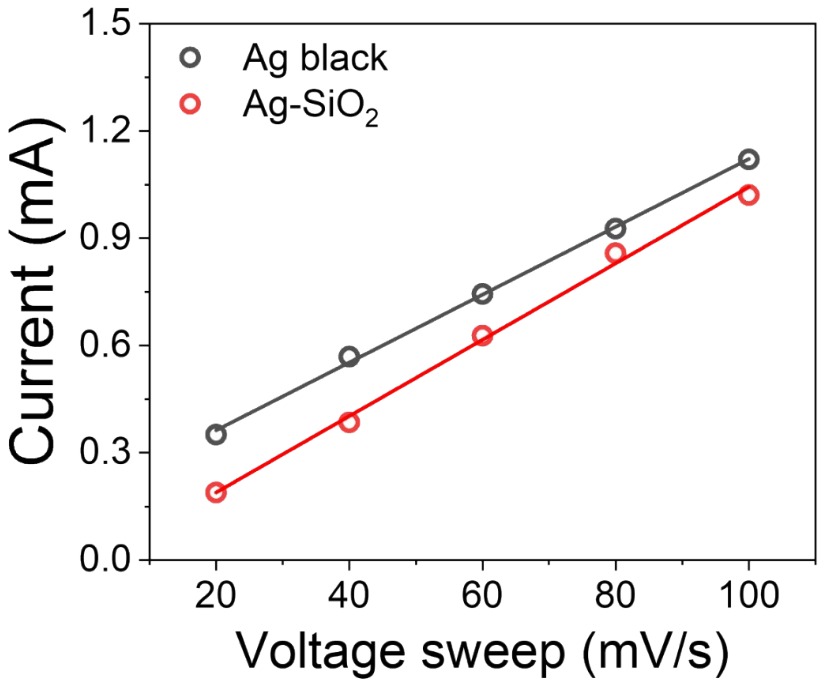

Fig. S11 Linear fitting of the capacitive currents versus CV scan rates of Ag black and Ag-SiO_2 before CO_2 reduction reaction.

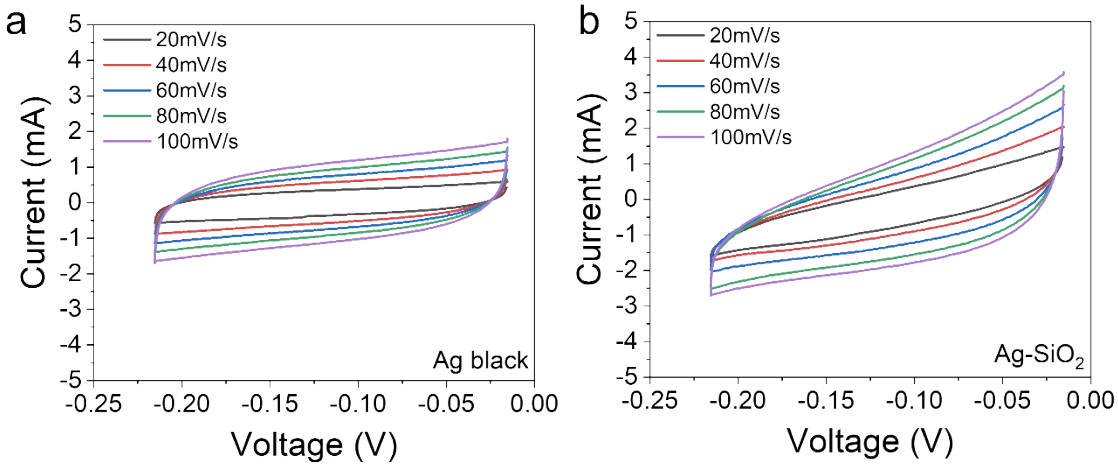

Fig. S12 ECSA of (a) Ag black and (b) Ag-SiO_2 before CO_2 reduction reaction.

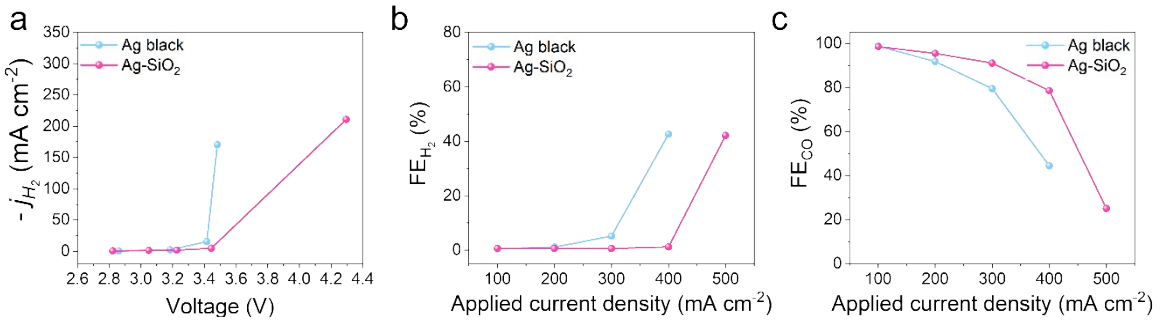

Fig. S13 CO_2RR performance of Ag black and Ag-SiO_2 in 0.1 M $KHCO_3$. (a) H_2 partial current density, (b) H_2 faradaic efficiency and (c) CO faradaic efficiency

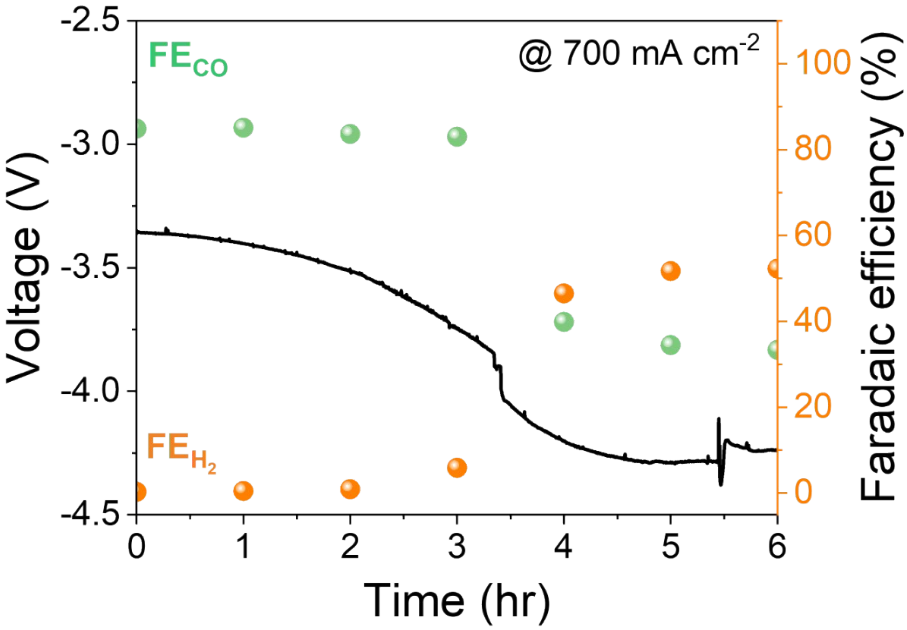

Fig. S14 The stability test of Ag black in 0.1 M $CsHCO_3$ using zero-gap CO2 electrolyzer at 700 mA cm^{-2}.

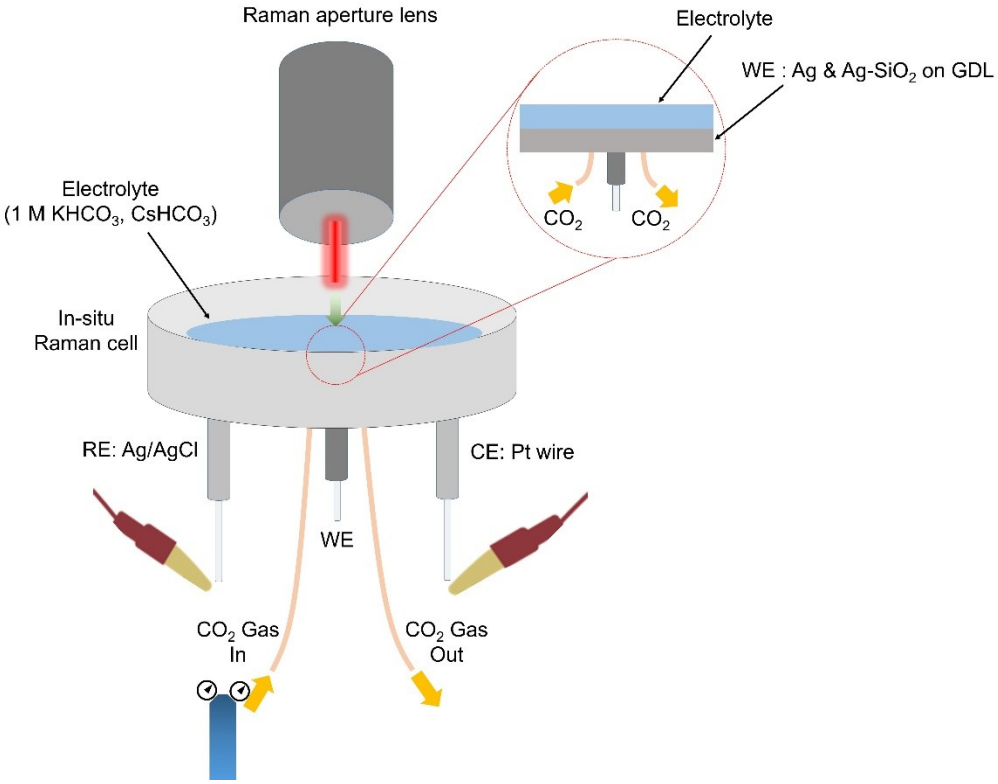

Fig. S15 A schematic depicting the experimental during in-situ/operando Raman spectroscopy.

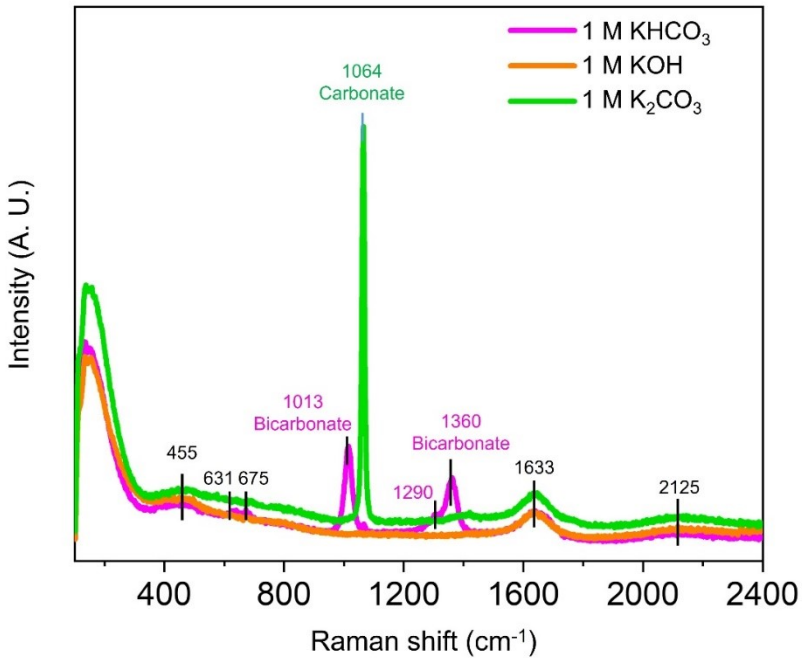

Fig. S16 Raman spectra of 1 M $KHCO_3$, 1 M KOH, and 1 M K_2CO_3 reference solutions.

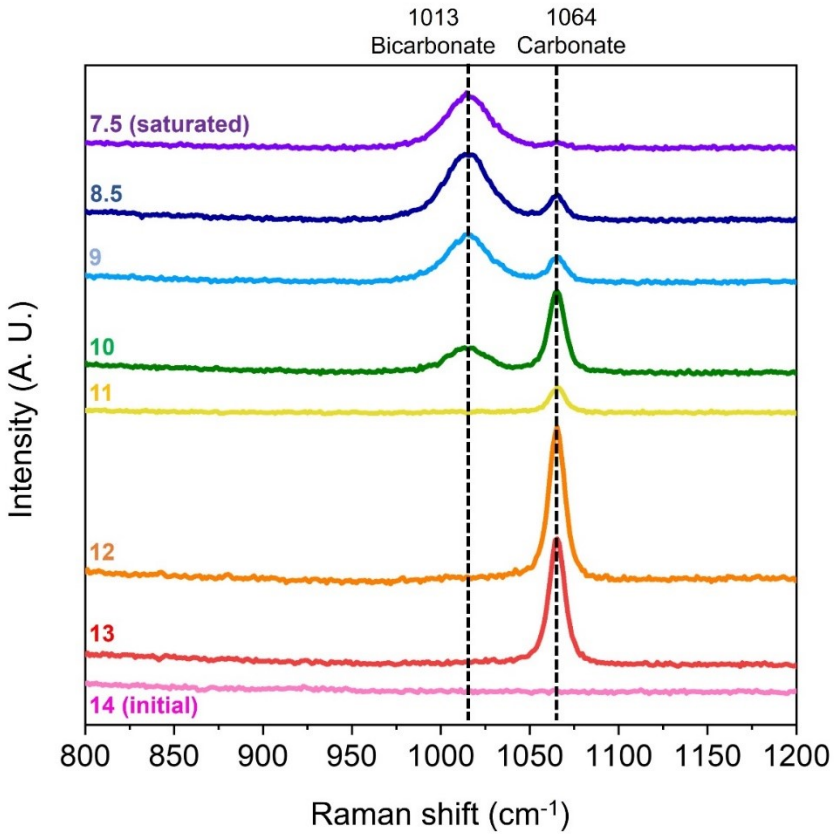

Fig. S17 Raman spectra of CO_2-purged, SiO_2-dissolved 1 M KOH solutions with varying pH values. After dissolving 90 mg of pristine SiO_2 powder in 15 ml of 1 M KOH solution (initial pH 14), CO_2 purging (100 ml/min) time was differed, until each solution reached a specific pH value while the solution pH was measured real time using a commercial pH meter.

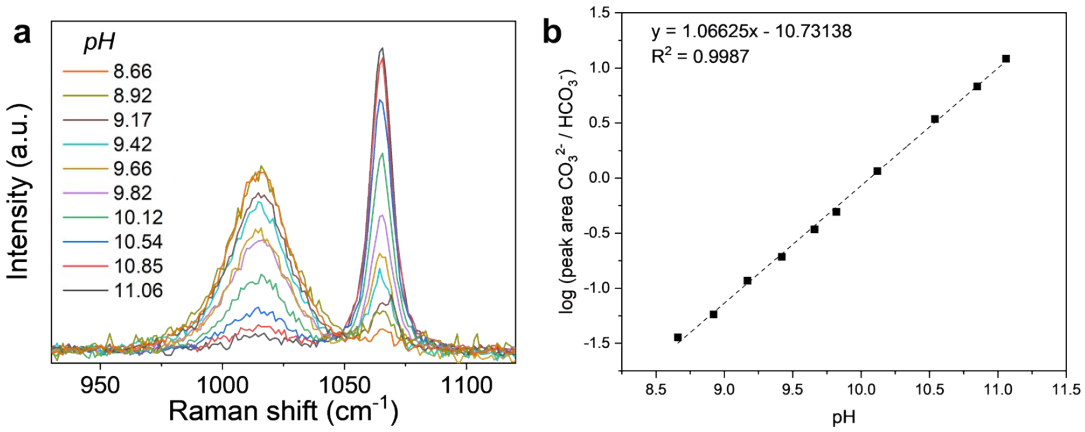

Fig. S18 (a) SERS spectra of various pH values by mixing KOH and $KHCO_3$ totaling 1M electrolyte. (b) Calibration results correlating the pH values of the solutions, and the relative peak area ratio of carbonate (denoted as I_C, 1064 cm^{-1}) to bicarbonate (denoted as I_B, 1013 cm^{-1}) by log-transforming. Solutions with pH values in the range of 8.66 – 11.06 were used only, as other solutions with pH values higher than 12 did not show peaks corresponding to bicarbonate peaks.

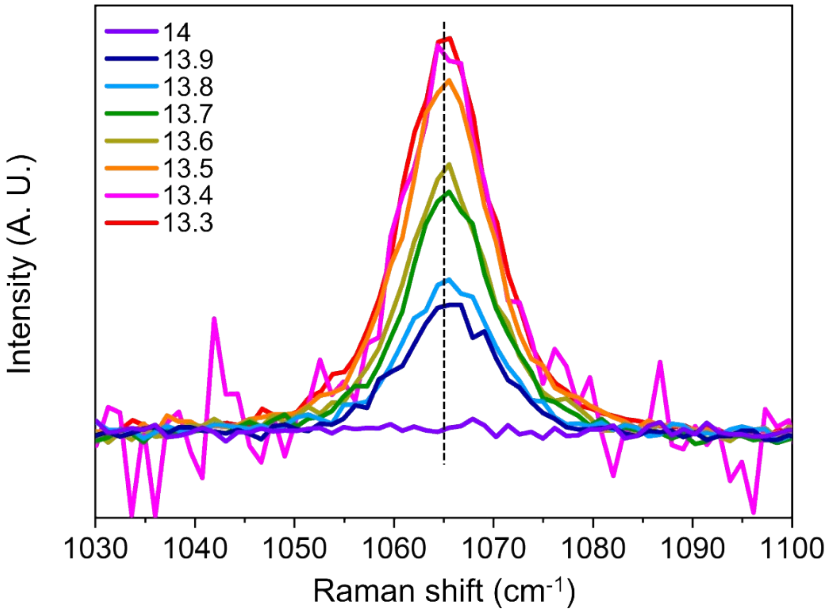

Fig. S19 Raman spectra of various KOH/$KHCO_3$ mixed solutions with varying pH solution values in the range of 13 – 14. 1 M KOH and 1 M $KHCO_3$ solutions were mixed in different ratios to prepare the solutions with different pH values. In case of pH 14 solution, pure 1 M KOH was used, without any 1 M $KHCO_3$ addition.

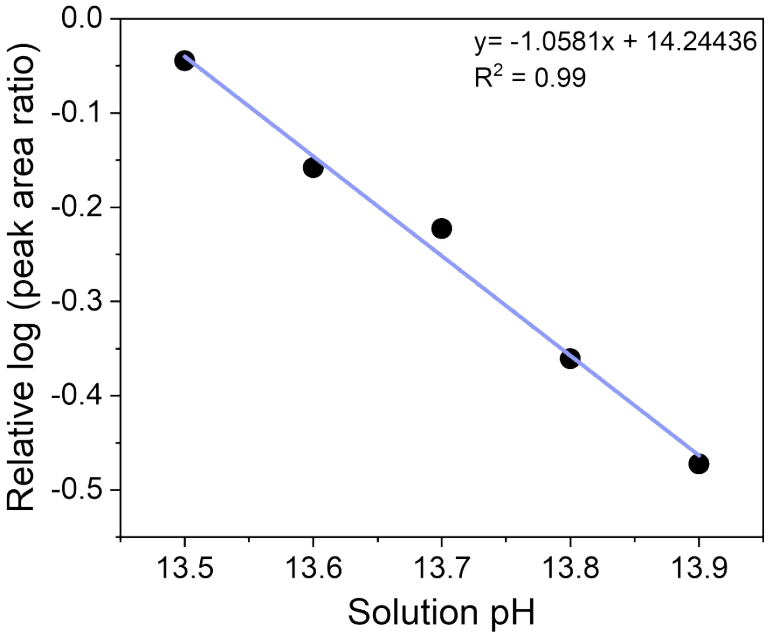

Fig. S20 Calibration results correlating the pH values of the 1 M KOH/$KHCO_3$ mixed solutions with pH values in the range of 13 – 14 M, and the relative log peak area ratios corresponding to carbonate (~1065 cm^{-1}) species shown in Supplementary Fig. 19. Raman peak area of carbonate species seen in pH 13.3 solution was set as reference.

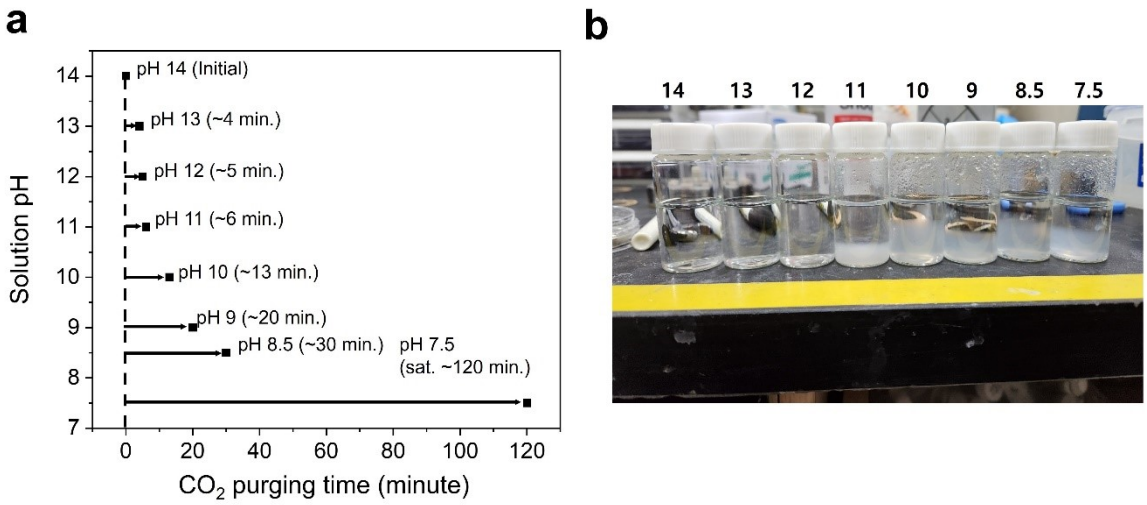

Fig. S21 (a) Change in solution pH of SiO_2-dissolved (90 mg) 1 M KOH solution (15 ml) plotted against a function of CO_2 purging time (100 ml/min). Solution pH was measured real time using a commercial pH meter, and (b) picture of CO_2-purged, SiO_2-dissolved 1 M KOH solutions with varying pH values in the range of 7.5 – 14. With sufficient CO_2 purging, an opaque gel within the solution is observable.

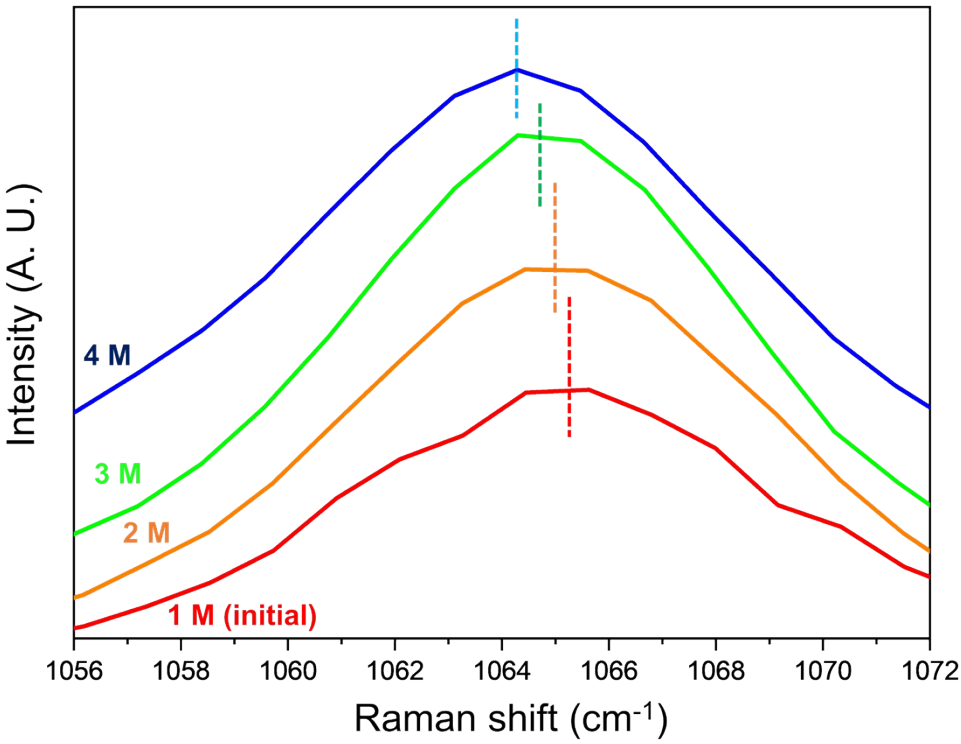

Fig. S22 Raman spectra of various KOH/$KHCO_3$ mixed solutions with varying K cation concentrations. Initially, a solution with pH value of 13.3 was prepared by mixing certain amounts of 1,2,3 and 4 M KOH and 1,2,3 and 4 M $KHCO_{3,}$ respectively.

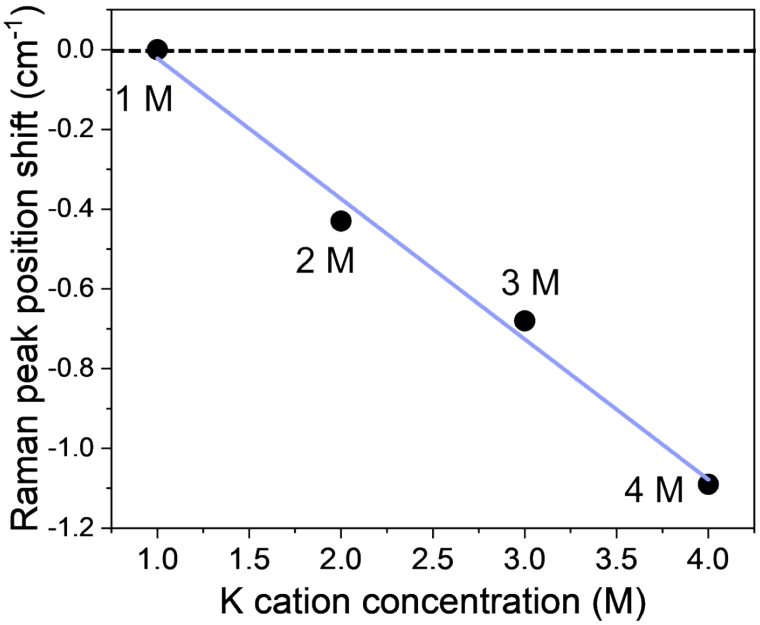

Fig. S23 Calibration results correlating the K cation concentrations of the solutions with K cation concentrations in the range of 1 – 4 M, and the peak position shifts corresponding to carbonate (~1065.38 cm^{-1}) Raman peaks shown in Supplementary Fig. 22.

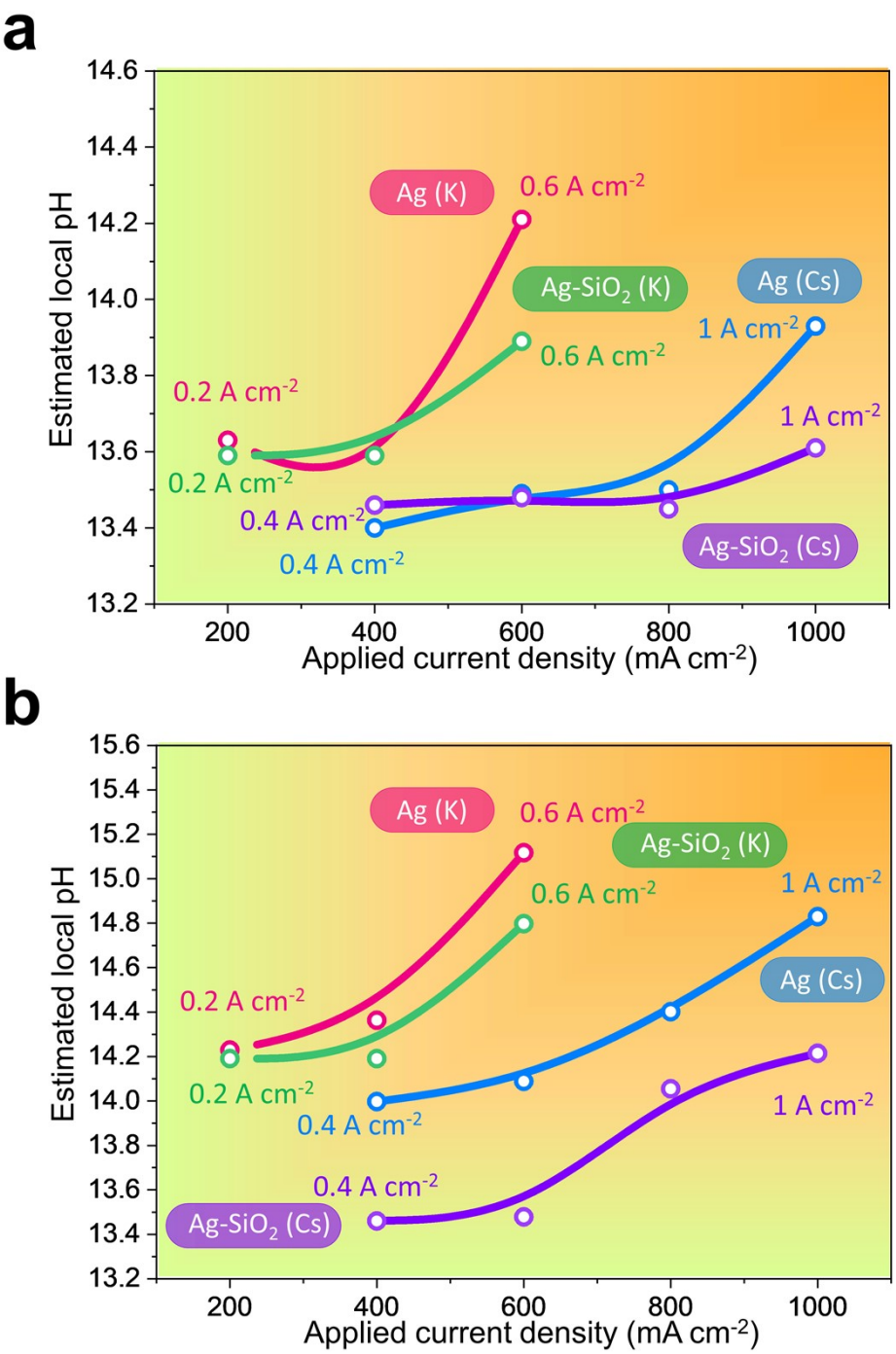

Fig. S24 Estimated local pH values based on in-situ/operando Raman using calibration curve in S20 and S23. (a) Estimated local pH without considering K concentration calibration. (b) Estimated local pH considering K concentration calibration. Reference points for peak shift and intensity: $KHCO_3$: 100 mA cm^{-2}, $CsHCO_3$: 200 mA cm^{-2}. At reference point, we assumed that pH is close to pH 13.

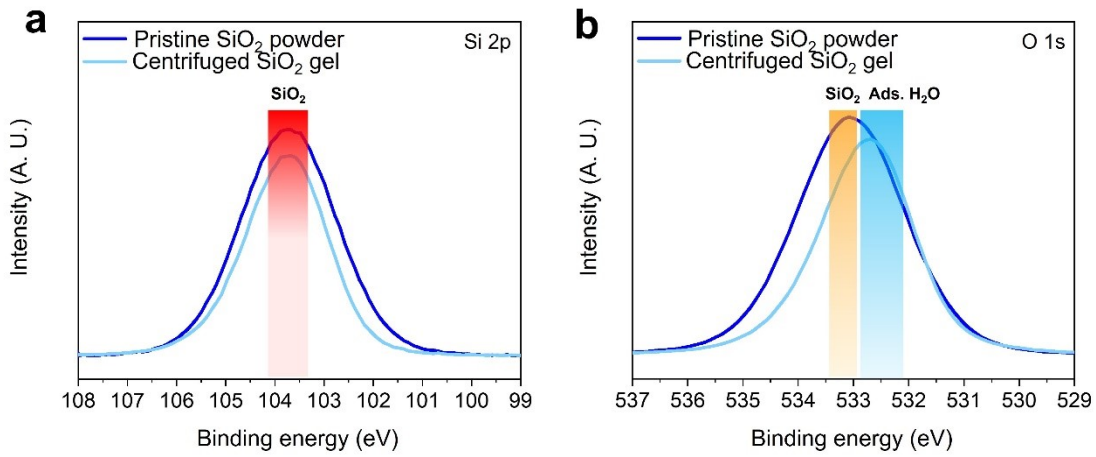

Fig. S25 XPS spectra of pristine SiO_2 powder and centrifuged SiO_2 gel in (a) Si 2p level and (b) O 1s level. All XPS spectra were calibrated by using C 1s peak (284.8 eV) as a reference. To obtain the centrifuged SiO_2 gel, 90 mg of SiO_2 powder was dissolved in 15 ml of 1 M KOH solution. After purging the solution with CO_2 (100 ml/min), an opaque gel was obtained within the solution. Then the solution was centrifuged (12000 rpm, 10 minutes) using D.I. water for 3 times. The obtained gel was then dried overnight in a convection oven (60 °C).

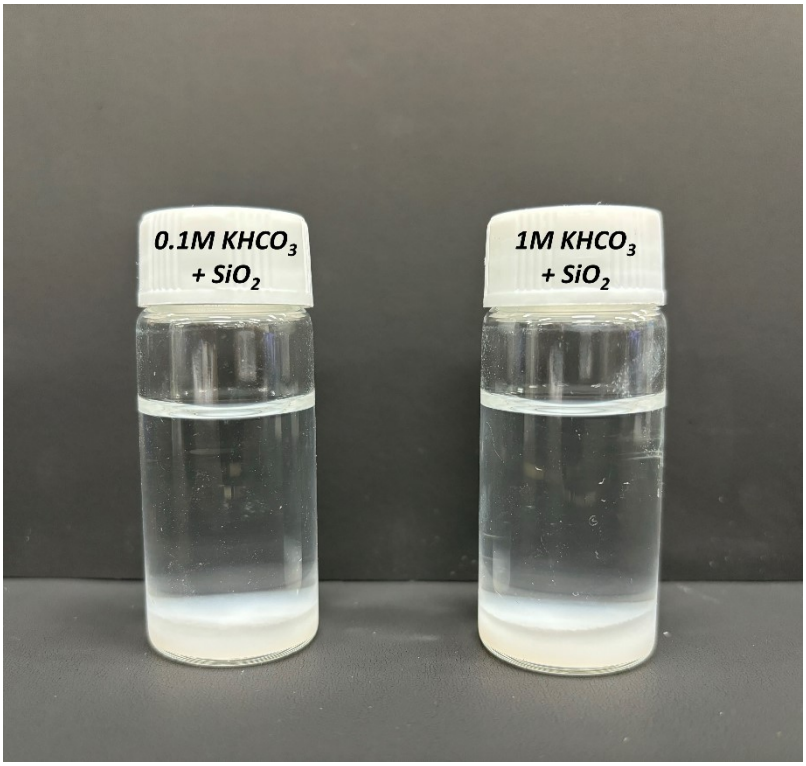

Fig. S26 SiO_2 (90 mg) dissolved in 0.1 M $KHCO_3$ and 1 M $KHCO_3$ (15 mL).

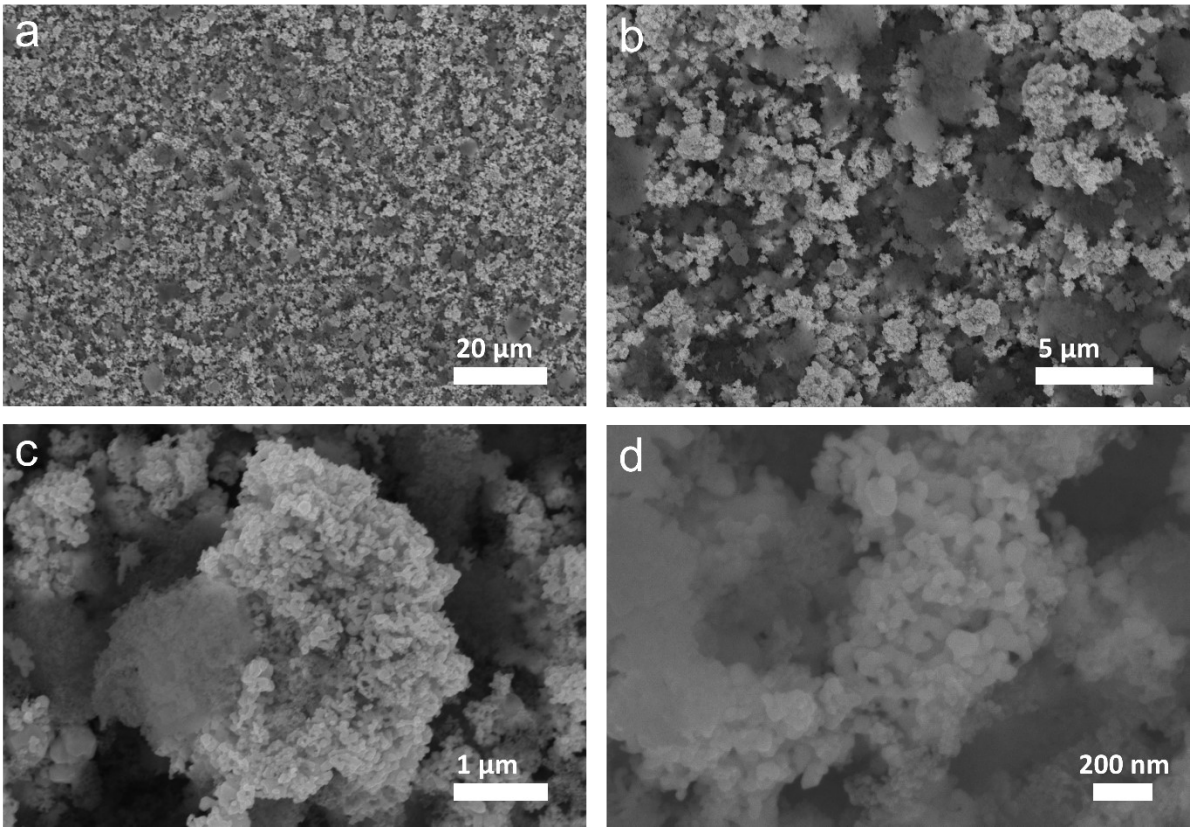

Fig. S27 SEM images of Ag-SiO_2 before CO_2 reduction reaction. (a, b) low-magnification and (c, d) high-magnification.

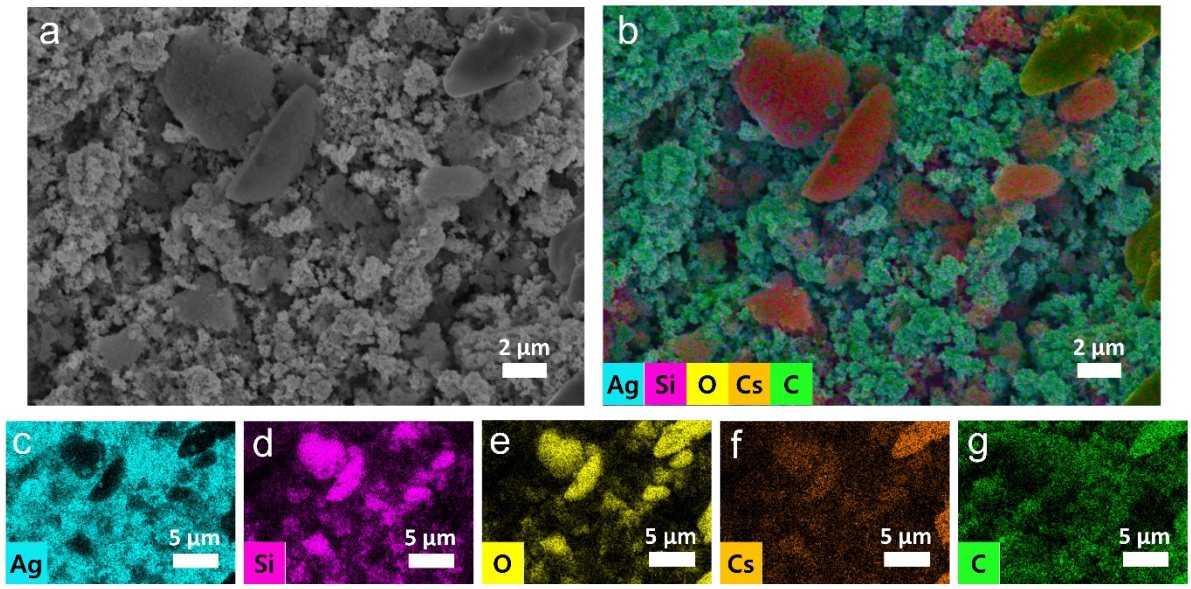

Fig. S28 (a) SEM image of Ag-SiO_2 after CO_2 reduction reaction at 200 mA cm^{-2} for 20 min. (b) SEM-EDS elemental mapping of the distribution of (b) overall of Ag, Si, O, Cs and C, (c) Ag, (d) Si, (e) O, (f) Cs and (g) C.

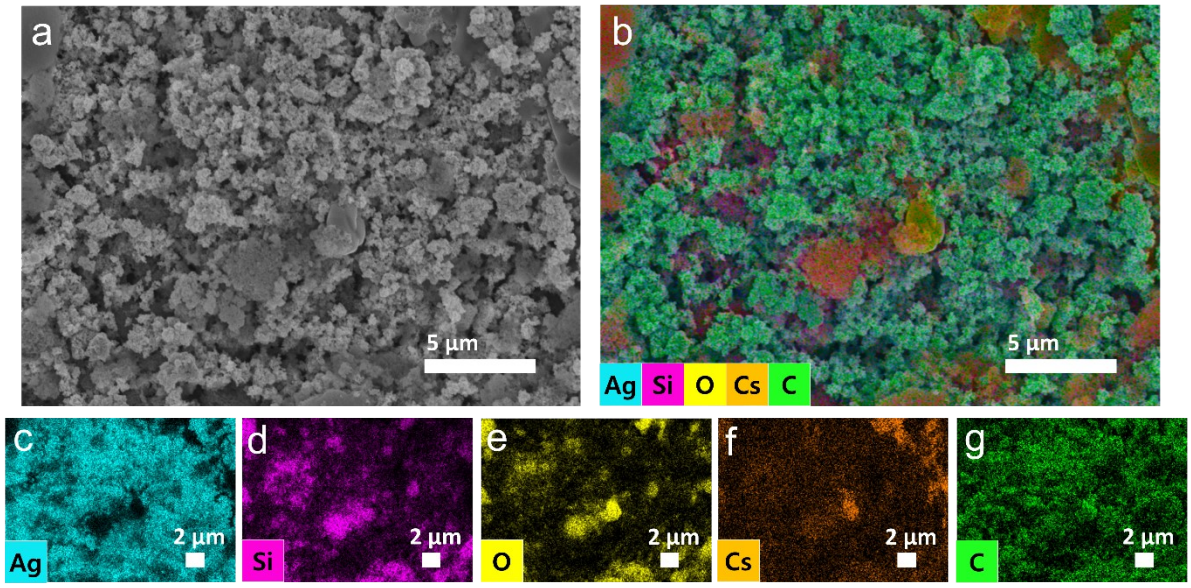

Fig. S29 (a) SEM image of Ag-SiO_2 after CO_2 reduction reaction at 500 mA cm^{-2} for 20 min. (b) SEM-EDS elemental mapping of the distribution of (b) overall of Ag, Si, O, Cs and C, (c) Ag, (d) Si, (e) O, (f) Cs and (g) C.

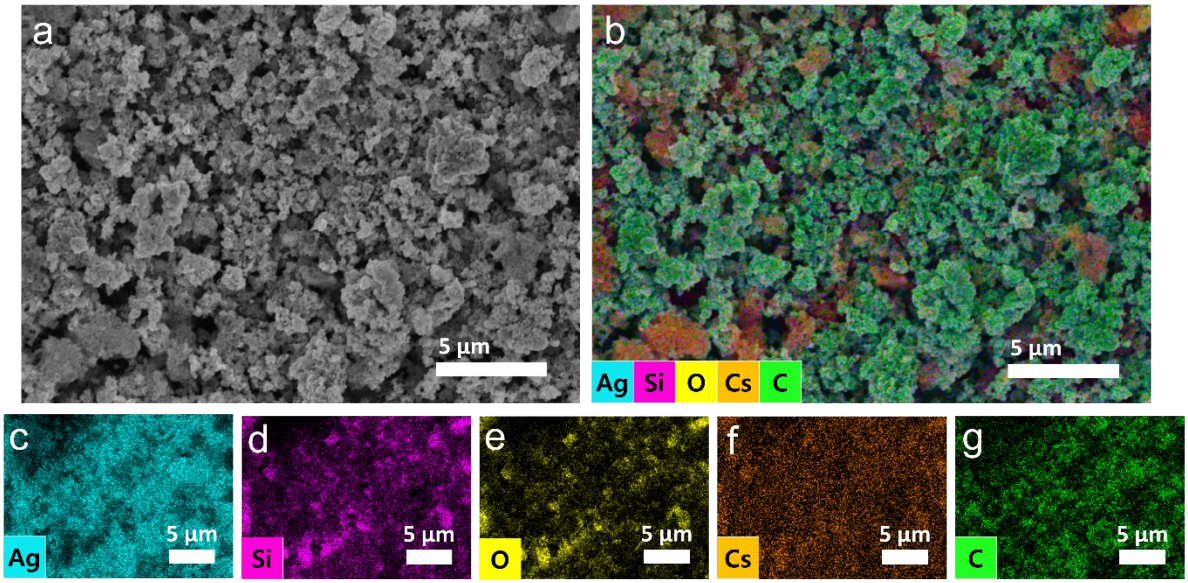

Fig. S30 (a) SEM image at 5000x magnification. of Ag-SiO_2 after CO_2 reduction reaction at 900 mA cm^{-2} for 20 min. (b) SEM-EDS elemental mapping of the distribution of (b) overall of Ag, Si, O, Cs and C, (c) Ag, (d) Si, (e) O, (f) Cs and (g) C.

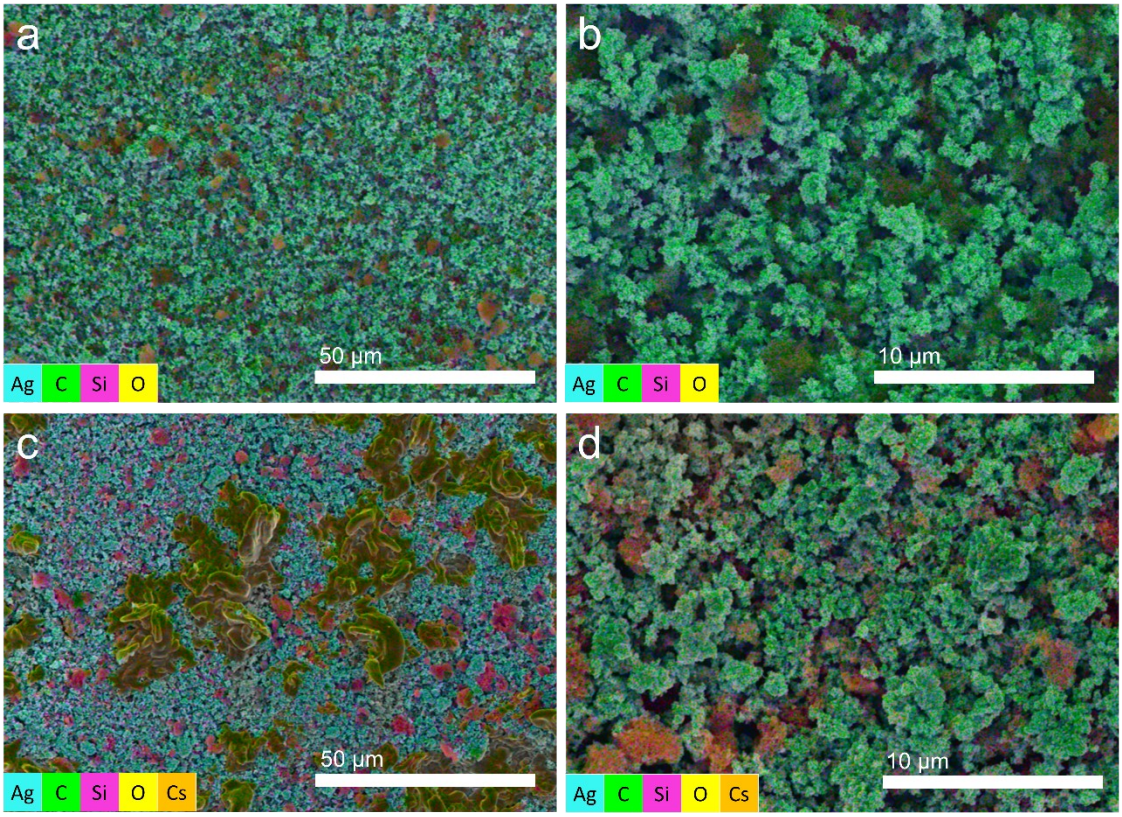

Fig. S31 Ag-SiO_2 EDS images of low magnification. (a, b) before reaction and (c, d) after reaction with 900 mA cm^{-2}.

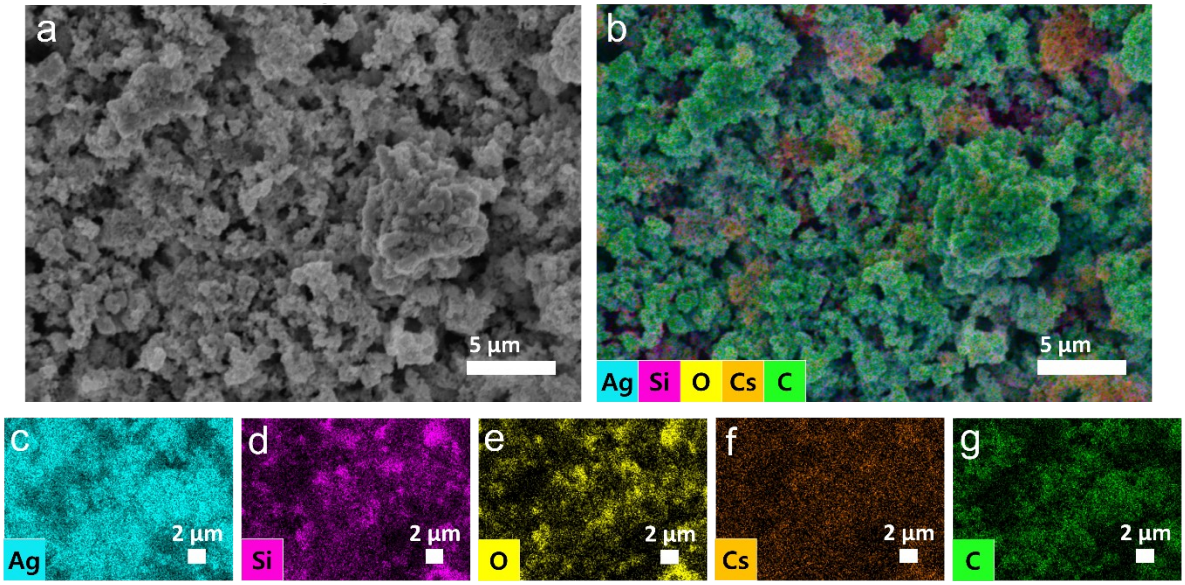

Fig. S32 (a) SEM image at 10000x magnification of Ag-SiO_2 after CO_2 reduction reaction at 900 mA cm^{-2} for 20 min. (b) SEM-EDS elemental mapping of the distribution of (b) overall of Ag, Si, O, Cs and C, (c) Ag, (d) Si, (e) O, (f) Cs and (g) C.

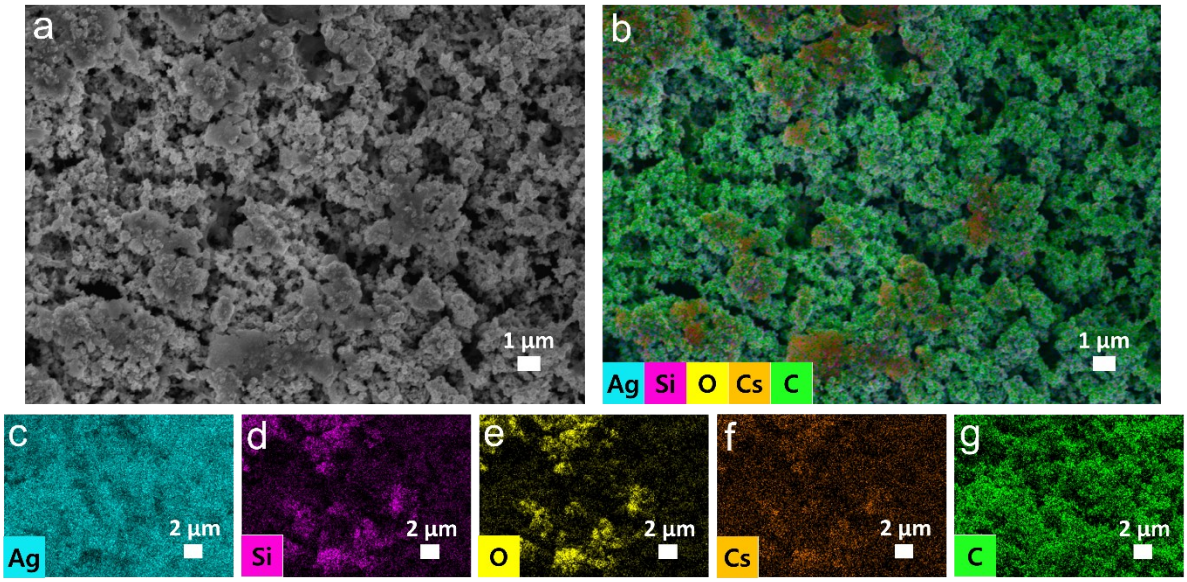

Fig. S33 (a) SEM image of Ag-SiO_2 supplied with CO_2 during 20 min after CO_2 reduction reaction at 900 mA cm^{-2} for 20 min. (b) SEM-EDS elemental mapping of the distribution of (b) overall of Ag, Si, O, Cs and C, (c) Ag, (d) Si, (e) O, (f) Cs and (g) C.

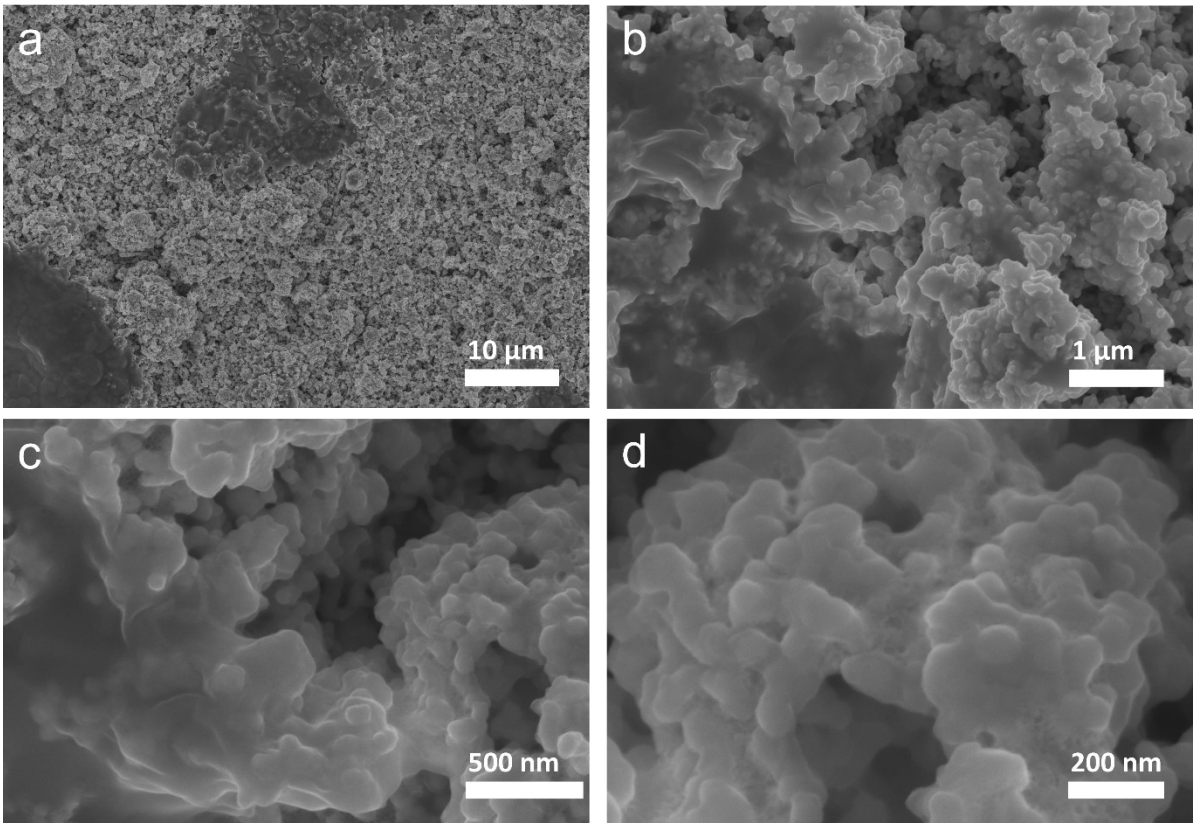

Fig. S34 SEM images of Ag black after CO_2 reduction reaction. (a, b) low-magnification and (c, d) high-magnification.

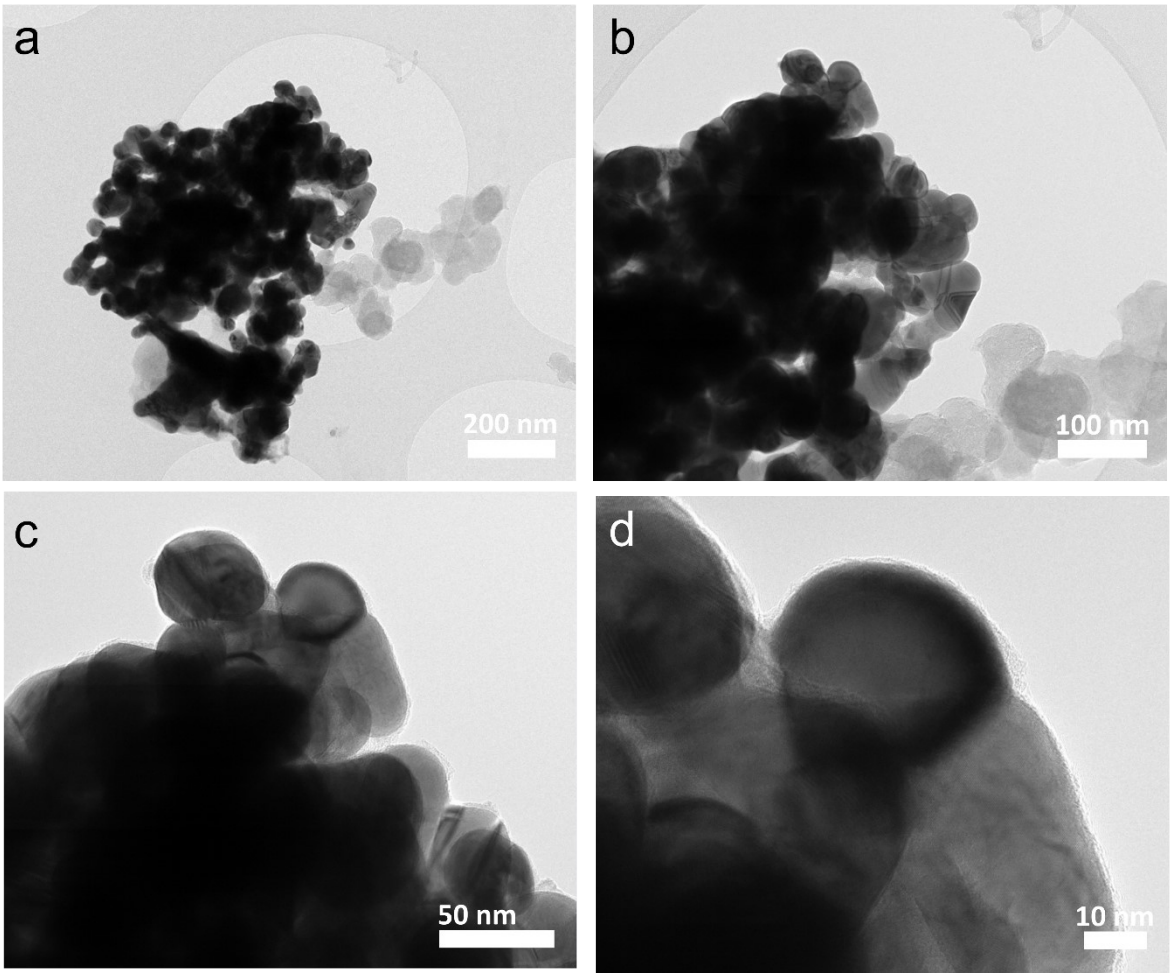

Fig. S35 HR-TEM images of Ag black after CO_2 reduction reaction. (a) low-magnification and (b), (c), (d) high-magnification.

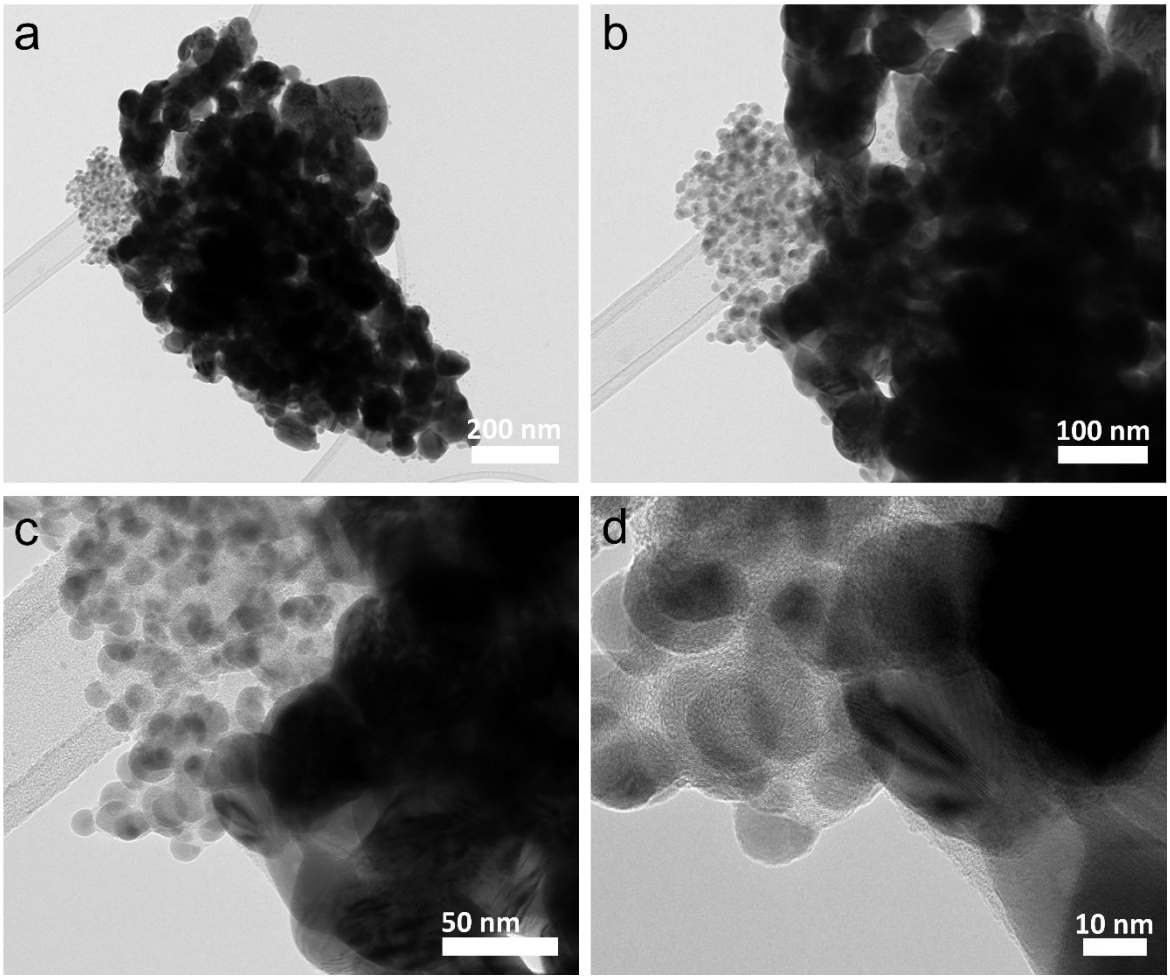

Fig. S36 HR-TEM images of Ag –SiO_2 after CO_2 reduction reaction. (a) low-magnification and (b), (c), (d) high-magnification.

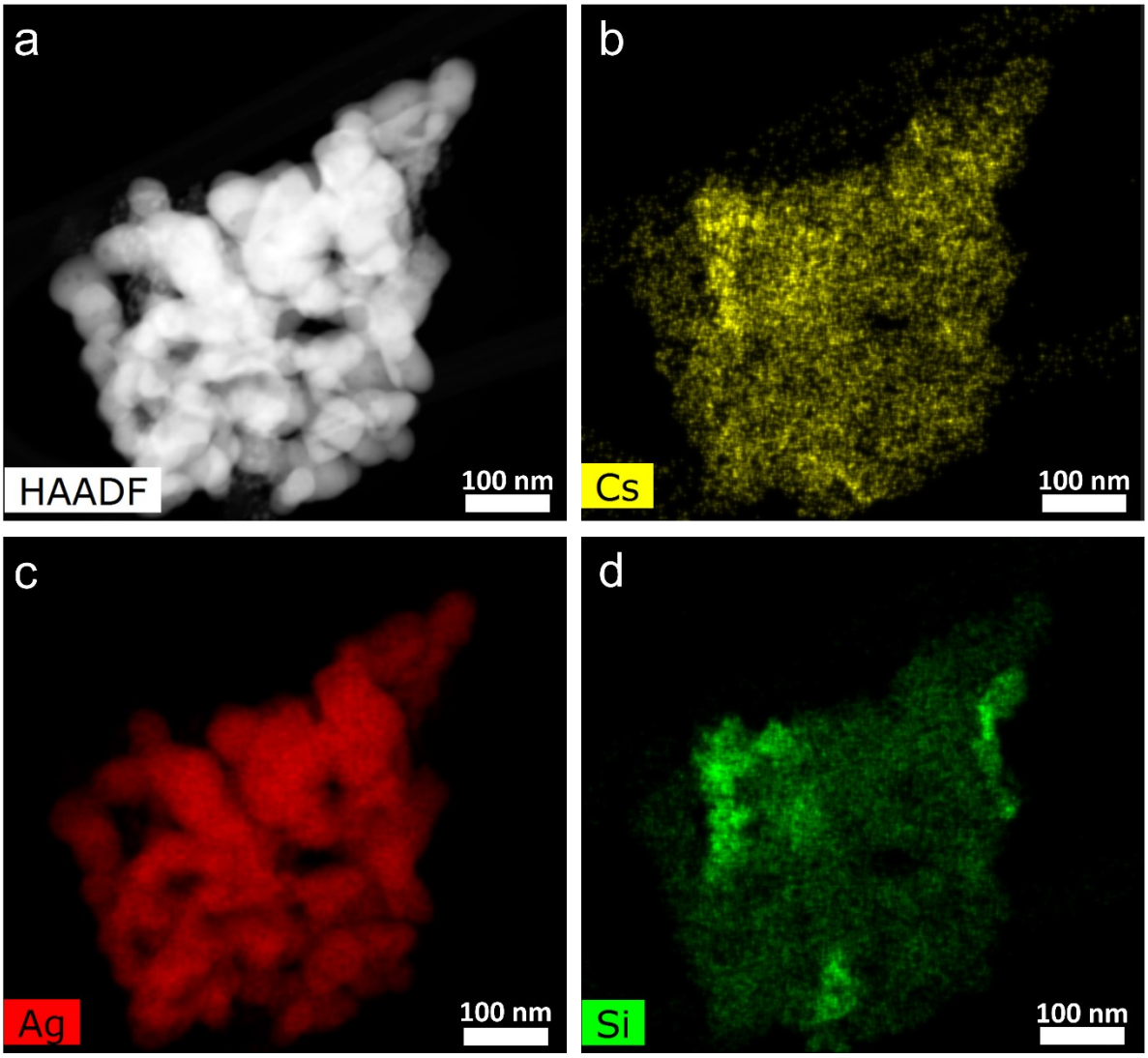

Fig. S37 (a) HAADF STEM image of Ag-SiO_2 after CO_2 reduction reaction. STEM-EDX elemental mapping of the distribution of (b) Cs, (c) Ag and (d) SiO_2.

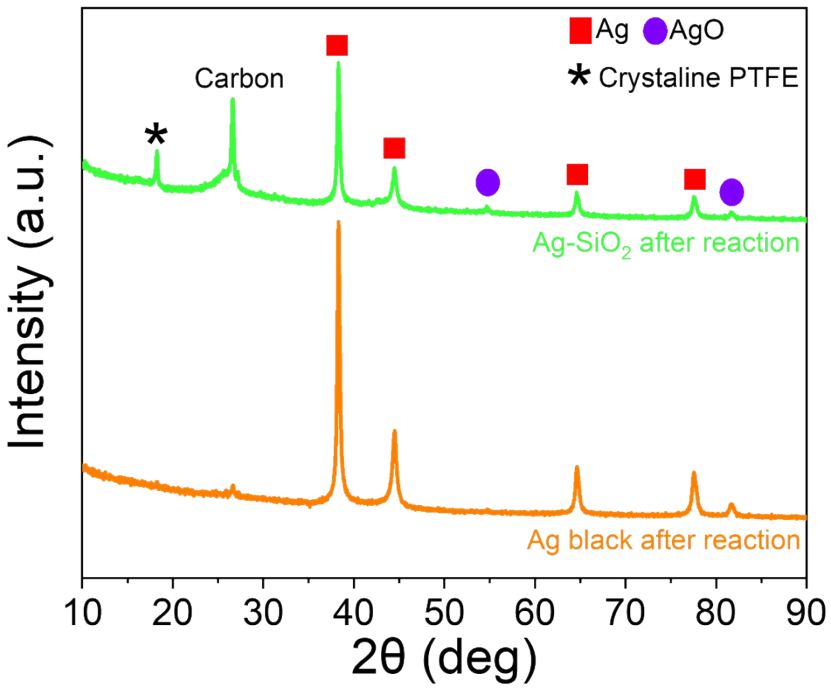

Fig. S38 XRD patterns of Ag black and Ag-SiO_2 after CO_2 reduction reaction.

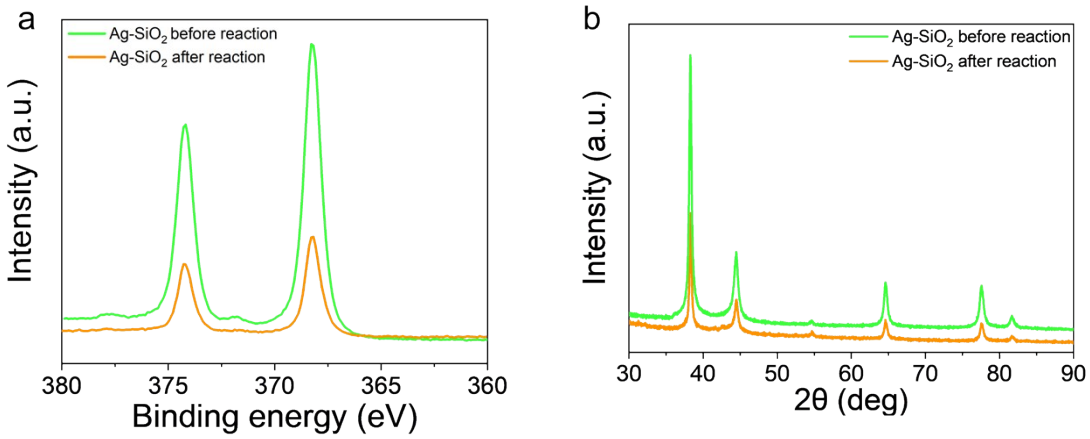

Fig. S39 (a) XPS results and (b) XRD profiles of Ag-SiO_2 before and after reaction.

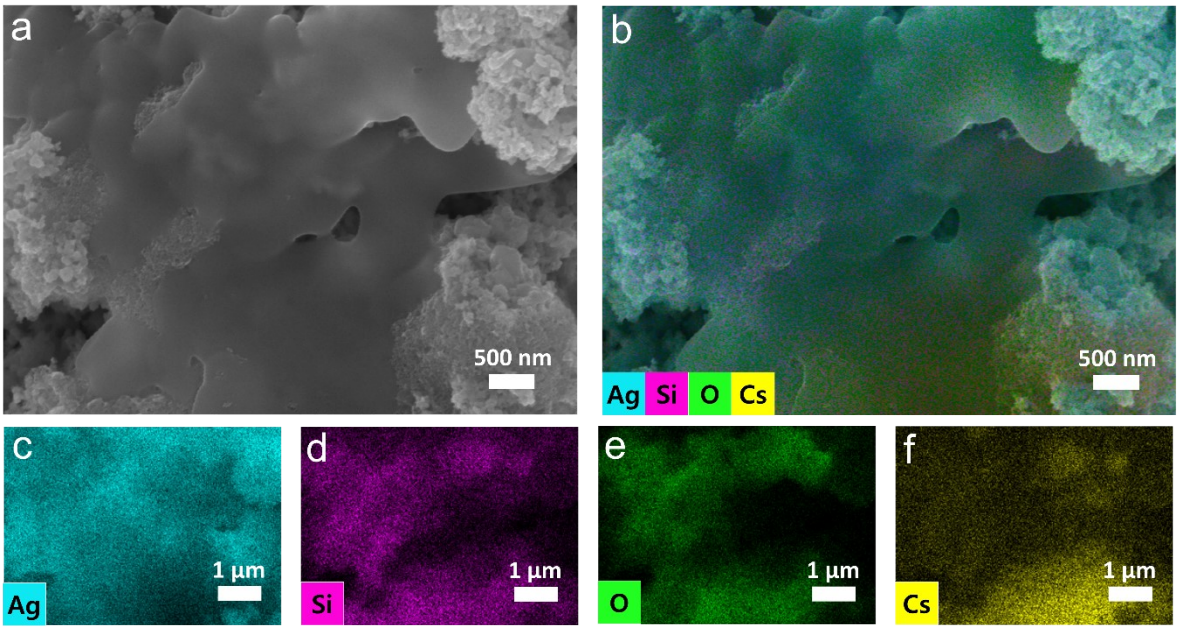

Fig. S40 (a) SEM image of Ag-SiO_2 after CO_2 reduction reaction at 800 mA cm^{-2} for 2 h. (b) SEM-EDS elemental mapping of the distribution of (b) overall of Ag, Si, O, Cs and C, (c) Ag, (d) Si, (e) O and (f) Cs.

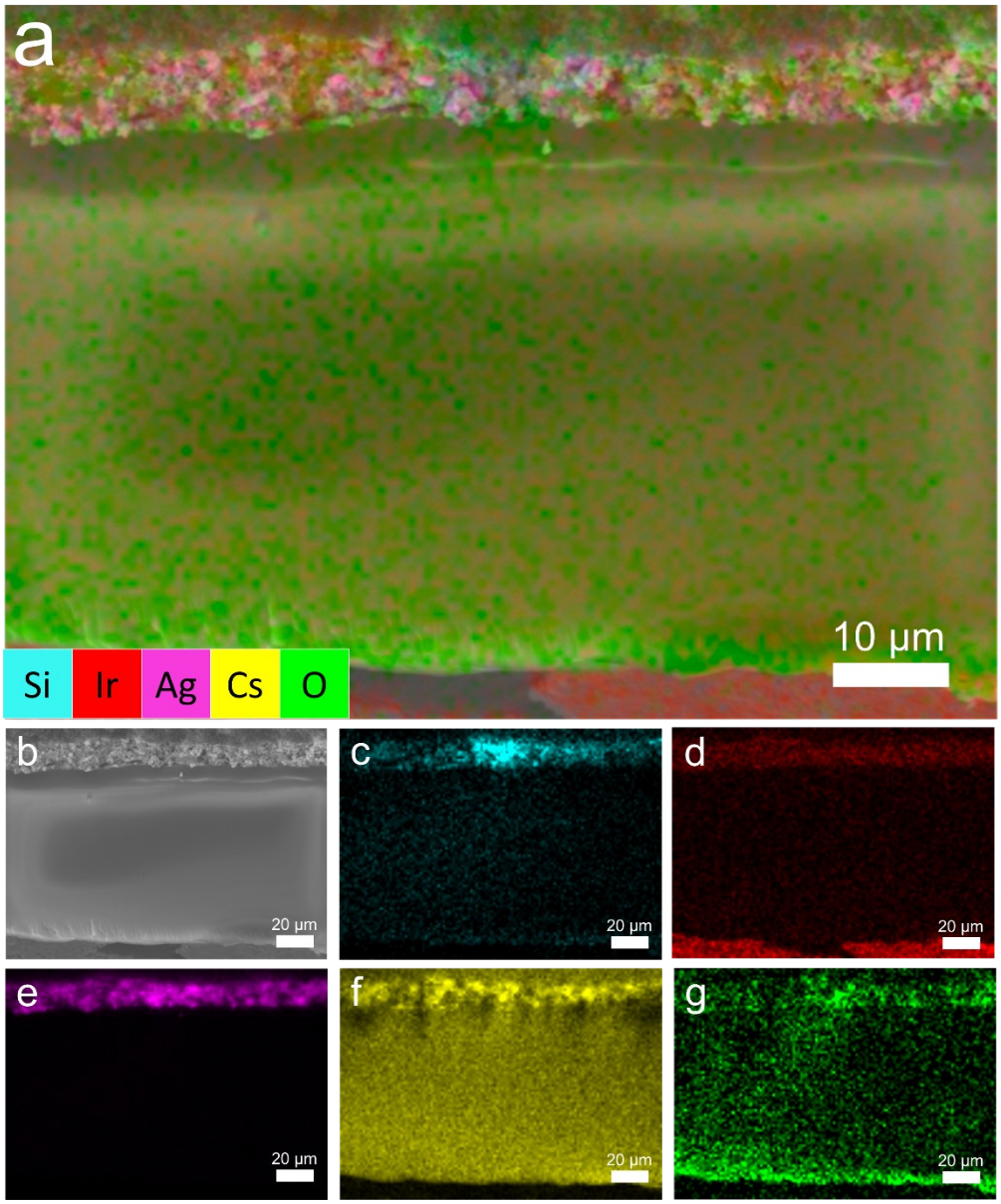

Fig. S41 Cross-section images of AEM after CO_2 reduction reaction at 700 mA cm^{-2} for 1h. (a) SEM-EDS elemental mapping overall of AEM, (b) SEM image of AEM, SEM-EDS elemental mapping of the distribution of (c) Si (d) Ir, (e) Ag, (f) Cs and (g) O.

Table S1. Estimated local pH values based on in-situ/operando Raman using calibration curve in S20 and S23. Reference points for peak shift and intensity: $KHCO_3$: 100 mA cm^{-2}, $CsHCO_3$: 200 mA cm^{-2}. At reference point, we assumed that pH is close to pH 13.

Sample	Current density (mA cm^{-2})	CO_3^{2-}/ CO_3^{2-} at reference (Area ratio)	Log (Area ratio)	Esitimated local pH	Estimated cation concentration	Esitimated local pH considering cation concentration
Ag-$KHCO_3$	200	0.6688	-0.1747	13.63	4M	14.22
	400	1.0048	0.0021	13.46	8M	14.36
	600	0.1601	-0.7955	14.21	8M	15.12
Ag-SiO_2 $KHCO_3$	200	0.7344	-0.1341	13.59	4M	14.06
	400	0.7350	-0.1337	13.59	4M	14.19
	600	0.3488	-0.4574	13.89	8M	14.79
Ag-$CsHCO_3$	400	1.1771	0.0708	13.40	4M	14.00
	600	0.9428	-0.0256	13.49	4M	14.09
	800	0.9152	-0.0385	13.50	8M	14.40
	1000	0.3228	-0.4911	13.93	8M	14.83
Ag-SiO_2 $CsHCO_3$	400	1.0053	0.0023	13.46	1M	13.46
	600	0.9612	-0.0172	13.48	1M	13.48
	800	1.0233	0.0100	13.45	4M	14.05
	1000	0.6935	-0.1590	13.61	4M	14.21

References

1. D. A. Henckel, M. J. Counihan, H. E. Holmes, X. Chen, U. O. Nwabara, S. Verma, J. Rodríguez-López, P. J. Kenis and A. A. Gewirth, *ACS Catalysis*, 2020, **11**, 255-263.